Results in Physics 87 (2026) 108719

Contents lists available at ScienceDirect

Results in Physics

journal homepage: www.elsevier.com/locate/rinp

DFT and experimental study of expired phenazopyridine doping PMMA for NLO and optical limiting applications

Raed K. Zaidan [a], Basil A. Abdullah [b,*], Mohammed T. Obeed [c], Abeer Mohammed Jabbar [d], Ali Qassim Abdullah [b]

[a] Chemistry Department, University of Basrah, Basrah, Iraq
[b] Physics Department, University of Basrah, Basrah, Iraq
[c] Department of Material Science, Polymer Research Centre, University of Basrah, Basrah, Iraq
[d] Department of Chemical and Petroleum Refining Engineering, College of Oil and Gas Engineering, Basrah University for Oil and Gas, Basrah, Iraq

ARTICLE INFO

Keywords:
Phenazopyridine
PMMA composite
Nonlinear optics
Optical limiting
DFT
Circular economy
Z-scan

ABSTRACT

Efficient organic nonlinear optical (NLO) material is of great interest for photonic and optoelectronic applications. The present work involved the doping of Phenazopyridine extracted from expired pharmaceutical tablets into poly(methyl methacrylate) (PMMA) to synthesize composite thin films of PMMA doped with 10, 30 and 50 wt% Phenazopyridine. FTIR, UV–Vis, ^{1}H NMR and ^{13}C NMR spectroscopy were used to confirm the chemical structure of the extracted compound. The electronic structure and optical properties were studied with the help of the density functional theory (DFT) and time dependent density functional theory (TD-DFT) methods at B3LYP/6–311 + G(d,p) and CAM-B3LYP/6–311 + G(d,p) levels of theory. The molecular orbitals calculated showed an efficient intramolecular charge-transfer character of Phenazopyridine with its donor–π–acceptor architecture. Open and closed aperture Z-scan methods were used to measure the nonlinear optical properties using continuous wave laser excitation at 532 nm. The composite films showed significant saturable absorption and saturable absorption index in the reverse direction, as well as negative nonlinear refraction, which showed self-defocusing properties. The nonlinear optical response was found to be higher at higher dye concentration, while the 50 wt% Phenazopyridine/PMMA film showed the highest nonlinear absorption coefficient and optical limiting performance. The nonlinear behavior observed is explained by the excited-state absorption and thermally induced nonlinear effects. The results indicate that Phenazopyridine/PMMA composites have interesting nonlinear optical properties and show that the use of outdated pharmaceutical drugs as functional materials in photonic applications seems promising.

Introduction

Nonlinear optical (NLO) materials have been the subject of great interest due to their potential applications in optical limiting, optical switching, signal processing, frequency conversion, data storage and photonic devices. With the growing need for new and improved optoelectronic technologies, intensive research efforts have focused on organic materials because of their high nonlinear optical susceptibilities, rapid response times, tunability, low costs, and ease of fabrication. Generally, organic chromophores tend to have greater intramolecular charge transfer (ICT) interactions than inorganic materials, that is, intramolecular charge transfer complexes are often stronger in organic chromophores than in inorganic materials, and are crucial for improving third-order nonlinear optical properties [1–3].

Azobenzene based dyes are an important class of NLO materials as they possess extended π-conjugated systems, high optical absorption and possess excellent charge transfer properties [4]. Since the presence of the azo linkage (–N=N–) allows electron delocalization between the electron donating and electron accepting groups, there is an improvement in the nonlinear absorption and refractive properties [5]. In addition, azo compounds exhibit excellent photostability, structural tunability, and compatibility with polymeric matrices, making them attractive candidates for photonic, optoelectronic, and nonlinear optical applications.[6].

Incorporation of organic dyes into polymer matrices is a good way to achieve mechanical stability, processability, and optical properties of

* Corresponding author.
E-mail address: basil.abdullah@uobasrah.edu.iq (B.A. Abdullah).

https://doi.org/10.1016/j.rinp.2026.108719
Received 28 April 2026; Received in revised form 7 June 2026; Accepted 23 June 2026
Available online 25 June 2026

NLO materials [7]. Poly(methyl methacrylate) (PMMA) is one of the most used host polymers because of its good transparency in the visible region, low optical losses and environmental stability, and easy film formation [8]. Dye doped PMMA composites are materials with the desired physical properties along with a strong nonlinear optical response of the dye molecules suitable for optical limiting or laser protection applications [9].

Phenazopyridine is an electron rich azo pharmaceutical compound with an amino substituted electron rich aromatic ring linked to a pyridine fragment by an azo bridge, which represents a donor–π–acceptor (D–π–A) molecular architecture. This kind of structure can be beneficial for intramolecular charge transfer and could be beneficial for the presence of noticeable nonlinear optical effect. Phenazopyridine has been extensively studied for its pharmaceutical usage but its nonlinear optical properties are not explored to a large extent. However, there are very few studies on the nonlinear absorption, nonlinear refraction, optical limiting properties and theoretical electronic structure of polymer composites based on Phenazopyridine [10].

Furthermore, the benefit of using expired pharmaceutical compounds as functional optical materials provides an attractive pathway to valorization of pharmaceutical wastes and sustainable materials development. Often, expired drugs are thrown away, even though they have physically useful molecular structures [11]. Their potential application in the field of photonic applications can be investigated as an environmentally friendly solution to waste conversion to valuable functional materials in the field of pharmaceutical processing [12].

Keeping these in mind, the present work aims at exploring the nonlinear optical characteristics of Phe obtained from expired pharmaceutical tablets and introduced to PMMA thin-film. To assure the chemical integrity of the extracted compound, the molecular structure and electronic properties were examined using FTIR spectroscopy, UV–Vis spectroscopy, DFT and TD-DFT calculation, and also, the ^{1}H NMR and ^{13}C NMR were performed. The nonlinear optical property has been investigated experimentally via open- and closed-aperture Z-scan and diffraction-ring measurements, and optical limiting experiments under continuous-wave laser excitation. The experimental and theoretical studies enable the understanding of the structure–property relationships and understand the optical response of Phenazopyridine and its use as a low-cost organic NLO material for photonic and optoelectronic applications.

2. Experimental methods

2.1. Extraction and Sample Preparation

Phenazopyridine free base was extracted by dissolving the out-of-date tablets (10 x 100 mg) in 100 mL of and 10% aqueous NaOH was added. The free base was extracted using ethyl acetate (2 x 50 mL) and evaporated under low pressure to obtain the phenazopyridine (70% recovery; m.p. 136–137 °C), the recovered Phenazopyridine was preliminarily examined by thin-layer chromatography (TLC), which showed a single dominant spot under the employed chromatographic conditions, indicating the successful isolation of the target compound. Further structural confirmation was obtained using FTIR, ^{1}H NMR, and ^{13}C NMR analyses. [13].

In the case of thin film fabrication, 10^{-4} M solution of phenazopyridine was prepared in chloroform, and PMMA (0.3 g) in 5 mL of the same solution. Phenazopyridine-PMMA mixtures were prepared at 10%, 30% and 50% weight percent (wt.%) and then the mixtures were drop-casted onto glass surfaces using the drop-casting method. The substrates were washed with acetone then distilled water before deposition to assure a homogeneous surface that was contaminant-free. All preparation parameters were kept under strict control to achieve uniformity and reproducibility of the films, such as maintaining a constant concentration of the solution, the same conditions of deposition, and ambient conditions. The films were left to dry at room temperature under the same conditions of 72 h, and uniform smooth and defect free thin films were obtained. The prepared films were determined to be approximately 60 μm thick confirming the consistency of the deposition process and suitability for reliable optical measurements [14–16].

2.2. Characterization

Thin layer chromatography (TLC), Fourier transform infrared (FTIR), UV-Visible and nuclear magnetic resonance (NMR) studies were done to confirm the identity of the extracted Phenazopyridine and to determine its suitability for further optical studies. Initially TLC analysis was used to follow the extraction process and showed a single major component under the chromatographic conditions used. FTIR spectra were recorded using a PerkinElmer spectrometer in the range of 4000–400 cm^{-1} with a resolution of 1 cm^{-1}. UV–Vis absorption spectra were recorded by a Shimadzu double-beam spectrophotometer (Model 1900i) at the spectral resolution of 1 nm and in the spectral range of 150–1100 nm. Furthermore, its molecular structure was further confirmed by obtaining ^{1}H NMR and ^{13}C NMR spectra of the recovered compound. The spectroscopic analysis indicated the characteristic structural features of Phenazopyridine and the combined analyses were consistent, which supported successful recovery of the target compound.

2.3. Z-scan measurements

The Z-scan technique was employed to investigate the nonlinear absorption coefficient and nonlinear refractive index of phenazopyridine in both solution and thin film forms. A Gaussian continuous-wave (CW) laser beam was used to scan the moving sample through the focus of a lens, allowing analysis of the transmittance to determine both the nonlinear refractive index and absorption coefficient. A DPSS CW laser with a wavelength of 532 nm, beam waist of 24 μm, and intensity of 1 kW/cm^2 was employed, with a 10 cm focal length lens. As the cuvette thickness (1 mm) was smaller than the Rayleigh range (3.4 mm), the thin sample approximation was valid. Transmittance was measured with and without a 3 mm pinhole in a far-field configuration (linear transmitting 0.4 (using a photodetector, and the data were recorded and analyzed using Z-scan software[17].

3. Computational Details

The quantum chemical and NLO properties calculations in this work were predicted with the Gaussian 16 program package (Revision B.01) [18]. Geometry optimization and frequency calculations were performed using the B3LYP/6-311+g(d,p) and CAM- B3LYP /6-311+g(d,p) [19–21] and to visualize the molecule, Gauss View 6.1.1 program was employed[22] for geometry optimizations and ground-state electronic structure calculations, the B3LYP functional with 6-311+G(d,p) basis set was used as it offers an acceptable compromise between cost and precision for π-conjugated organic molecules. However, the energies of long-range charge-transfer excitations can be underestimated by traditional hybrid functionals like B3LYP. The calculation of the excited-state properties and electronic transitions were thus performed by the use of the CAM-B3LYP functional as well. The Owing to its long-range correction scheme, CAM-B3LYP is a more reliable method for the description of intramolecular charge-transfer processes and optical excitations, which are especially crucial in systems that include donor–π–acceptor units like Phenazopyridine. Thus, the B3LYP/CAM-B3LYP level is provides a comprehensive and reliable theoretical framework for investigating the structural, electronic, and nonlinear optical properties of the studied molecule. The TD-DFT scheme was used to understand the electronic and linear optical behavior of Phenazopyridine molecule. The hyperpolarizability calculations were done with above mentioned basis set via hybrid functional CAM-B3LYP[23,24]. The optimized bond lengths calculated using the B3LYP and CAM-B3LYP functionals are listed in Table 1. The corresponding bond

Table 1
Bond length for optimized structure of phenazopyridine by using DFT-B3LYB and CAM-B3LYP functions.

Bond length	B3LYP	CAM- B3LYP
C1 –- C2	1.4016	1.3952
C1 –- C6	1.3976	1.3915
C1 –- H17	1.0860	1.0852
C4 –- N7	1.4136	1.4174
N7 –- N8	1.2718	1.2567
N8 –- C9	1.3792	1.3803
C9 –- C10	1.4317	1.4291
C12 –- N13	1.2908	1.2823
C15 –- N14	1.3568	1.3536
C15 –- N16	1.3483	1.3498

angles are presented in Table 2, while the calculated dihedral angles are summarized in Table 3.

4. Results and Discussion

4.1. Density functional theory (DFT)

Density functional theory (DFT) calculations were performed to optimize the equilibrium geometry of Phenazopyridine using the B3LYP/6-311+G(d,p) and CAM-B3LYP/6-311+G(d,p) levels of theory. The optimized molecular structure is presented in Fig. 1. The molecule can be seen to have an approximate planar structure, which is confirmed by the dihedral angles C6-C5-C4-N7 (-179.998° at B3LYP -179.999° at CAM-B3LYP) and C5-C4-N7-N8 (179.994° / 179.998°). This planarity is explained by the existence of the azo bridge (–N=N–) that lengthens π-conjugation along the molecular backbone.

The azo bond length N7=N8 is calculated to be 1.2718 Å (B3LYP) and 1.2567 Å (CAM-B3LYP), consistent with a typical N=N double bond. The amino group (–NH_2) attached to C15 (C15–N16 = 1.3483 Å / 1.3498 Å) acts as a strong electron-donating group, while the nitrogen atom in the pyridine ring (N17) serves as the primary electron-accepting site, forming a donor–π–acceptor (D–π–A) system that promotes intramolecular charge transfer. The dipole moments are calculated as 3.015 D (B3LYP) and 2.765 D (CAM-B3LYP), which shows that the molecule is moderately polarized. Also, the polarizability (212.03 a.u., CAM-B3LYP) indicates a high sensitivity of the electronic response to the external electric fields. The fact that the first hyperpolarizability (β) is positive supports once again the large nonlinear optical (NLO) activity of the compound, making it an attractive optoelectronic device.

The optimized geometries are the true minima of the potential energy surface as was verified by the lack of imaginary frequencies. The minor differences that were observed in the geometric parameters of the two functionals can be explained by the fact that they treat the exchange-correlation effects differently especially the long-range corrections incorporated in the CAM-B3LYP functional which are more effective in describing the interactions of charge-transfer [25].

Table 2
Bond Angle for optimized structure of phenazopyridine by using DFT-B3LYB and CAM-B3LYP functions.

Bond Angle	B3LYP	CAM- B3LYP
H17 –- C1 –- C6	120.290	120.250
H21 –- C6 –- C5	119.773	119.810
H18 –- C2 –- C3	119.591	119.612
C3 –- C4 –- N7	125.458	125.049
C4 –- N7 –- N8	115.444	115.360
N7 –- N8 –- C9	116.353	116.517
N8 –- C9 –- C15	115.759	115.936
C9 –- C15 –- N16	122.245	122.593
N8 –- C9 –- C10	126.577	126.150
H22 –- C10 –- C11	120.952	120.971
C12 –- N13 –- H24	110.496	110.772

Table 3
Dihedral length for optimized structure of phenazopyridine by using DFT-B3LYB and CAM-B3LYP functions.

Dihedral Angle	B3LYP	CAM- B3LYP
C6 –- C5 –- C4 –- N7	−179.998	−179.999
C5 –- C4 –- N7 –- N8	179.994	179.998
N8 –- C9 –- C10 –- H22	0.00750	0.01440
C9 –- C15 –- N16 –- H27	0.07490	0.13470
H25 –- N14 –- C15 –- N16	0	0.00549
H24 –- N13 –- C12 –- C11	0	0.00029
H19 –- C3 –- C4 –- N7	0.00093	0
H21 –- C6 –- C5 –- H20	0.00021	0.00028
C1 –- C2 –- C3 –- C4	0	0
C9 –- C10 –- C11 –- C12	0.00120	0.00282

4.2. Vibrational Spectroscopic Interpretation

The FTIR spectrum of Phenazopyridine (see Fig. 2) has typical absorption bands that are in line with the molecular structure. The FTIR spectrum of Phenazopyridine exhibited a broad absorption band centered at 3400 cm^{-1} together with a sharp band at 3282 cm^{-1}, which are assigned to the asymmetric and symmetric N–H stretching vibrations of the primary amino group (–NH_2), respectively. The weak absorption bands observed in the 3000–2850 cm^{-1} region are attributed to aromatic C–H stretching vibrations. A strong absorption band at 1657 cm^{-1} is assigned to the C=N stretching vibration of the pyridine ring, with a possible contribution from N–H bending vibrations. The bands located at 1543 and 1514 cm^{-1} are attributed to the skeletal C=C stretching vibrations of the aromatic rings. The medium-intensity band observed at 1394 cm^{-1} is mainly associated with the azo (–N=N–) stretching vibration, confirming the presence of the azo linkage within the molecular structure.

Furthermore, the absorption bands in the 1200–1000 cm^{-1} region are assigned to C–N stretching and in-plane C–H bending vibrations, whereas the bands below 1000 cm^{-1} are attributed to out-of-plane C–H bending modes of the aromatic rings. These characteristic absorption bands are consistent with the expected molecular structure of Phenazopyridine. In general, the vibrational characteristics observed attest to the presence of the functional groups of interest and are in agreement with the optimized structure of the molecules. The presence of both electron-giving (–NH_2) and electron-accepting (pyridine nitrogen and azo group) functional groups also confirms the establishment of a donor–π–acceptor framework, which may be attributed to the increased intramolecular charge transfer and nonlinear optical response. The observed absorption bands are consistent with previously reported spectroscopic studies of Phenazopyridine and related azo-pyridine compounds reported in the literature [26].

4.3. Structural Verification Using ^1H NMR and ^{13}C NMR Spectroscopy

The extracted Phenazopyridine was also confirmed by ^1H NMR and ^{13}C NMR spectroscopy (Fig. 3 and 4). The ^1H NMR spectrum (400 MHz, DMSO-d6) exhibited characteristic resonances at δ 7.72–7.68 (m, 3H), 7.44 (t, J = 7.8 Hz, 2H), and 7.28 (td, J = 7.1, 1.3 Hz, 1H), corresponding to the aromatic proton environments of the phenyl and pyridine rings. Also, a resonance at δ 5.99 (d, J = 8.7 Hz, 1H) was noted and assigned to the amino substituted aromatic group. Chemical shifts and splitting patterns observed are consistent with the expected proton environments of Phenazopyridine.

The ^{13}C NMR spectrum (100 MHz, DMSO-d6) displayed resonances at δ 161.4, 154.1, 153.2, 138.4, 129.2, 128.1, 124.3, 121.4, and 100.3 ppm. The downfield signals located in the 153-161 ppm region were assigned to the carbon atoms that were affected by adjacent nitrogen atoms in the pyridine ring, while the other resonances were attributed to the aromatic carbon atoms of the conjugated phenyl–azo–pyridine framework. The carbon chemical shifts obtained are in good accord with

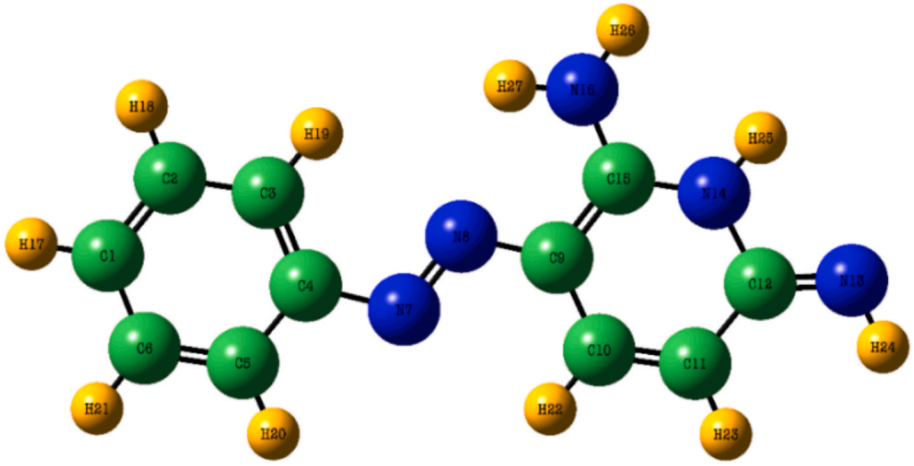

Fig. 1. Optimized geometry of phenazopyridine molecule.

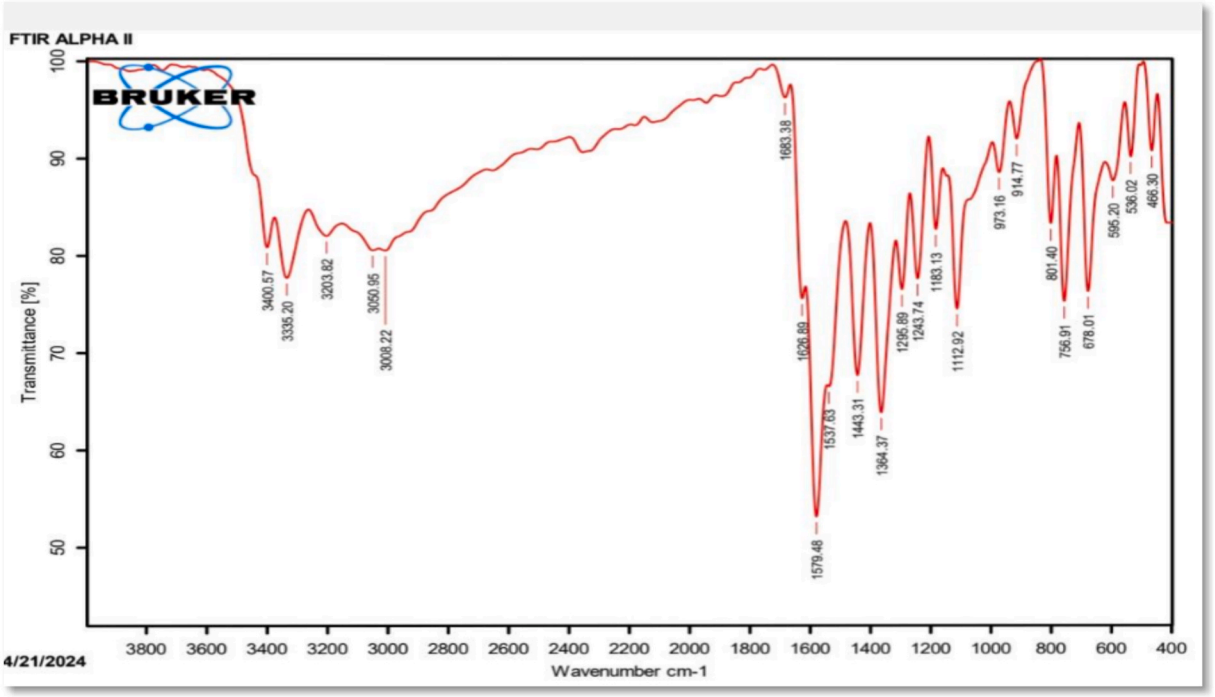

Fig. 2. FT-IR spectra of phenazopyridine molecule.

the proposed molecular structure.

The proton and carbon NMR spectra are in agreement with the molecular structure proposed for Phenazopyridine. The aromatic resonance in the δ 7.72–7.28 ppm region is attributed to protons of the phenyl and pyridine rings while the resonance at δ 5.99 ppm is assigned to the protons of the aminopyridine moiety. Typical ^{13}C NMR signals of the pyridine and phenyl carbon atoms in the conjugated phenyl–azo–pyridine framework was observed. There were no other strong resonances found, suggesting no significant degradation products were produced during extraction. The results obtained in combination with the FTIR and UV-Vis studies, indicate successful recovery and intactness of Phenazopyridine from the expired drug.

4.4. Absorption

Absorption properties of Phenazopyridine were experimentally studied in chloroform solution (0.1 mM) and PMMA-based thin films, and backed by theoretical computations based on TD-DFT/CAM-B3LYP. The spectrum of the experiment showed two clear bands, a visible peak at 430 nm, which is related to the n→π* transitions with some intramolecular charge-transfer (CT) character and a UV peak at 276 nm, which is related to the π→π*transitions. The experimental spectrum was found to be in good agreement with the simulated spectrum, indicating that the theoretical maximum of the spectrum was 424 nm, deviated by just 6 nm, which confirms the computational method Fig. 5a. The similarity between the experimental and simulated UV -vis spectrum was evaluated by comparing the location of the major absorption peaks. The minimal difference between the experimental and theoretical values of the peak wavelength (~6 nm) signifies the presence of a good degree of consistency in the two spectra. This result confirms that the computational model based on the DFT that uses the selected functional can reliably reproduce the electronic transitions of the system. The minor deviations between experimental and theoretical values can be explained by both environmental influences, e.g., solvent or solid-state

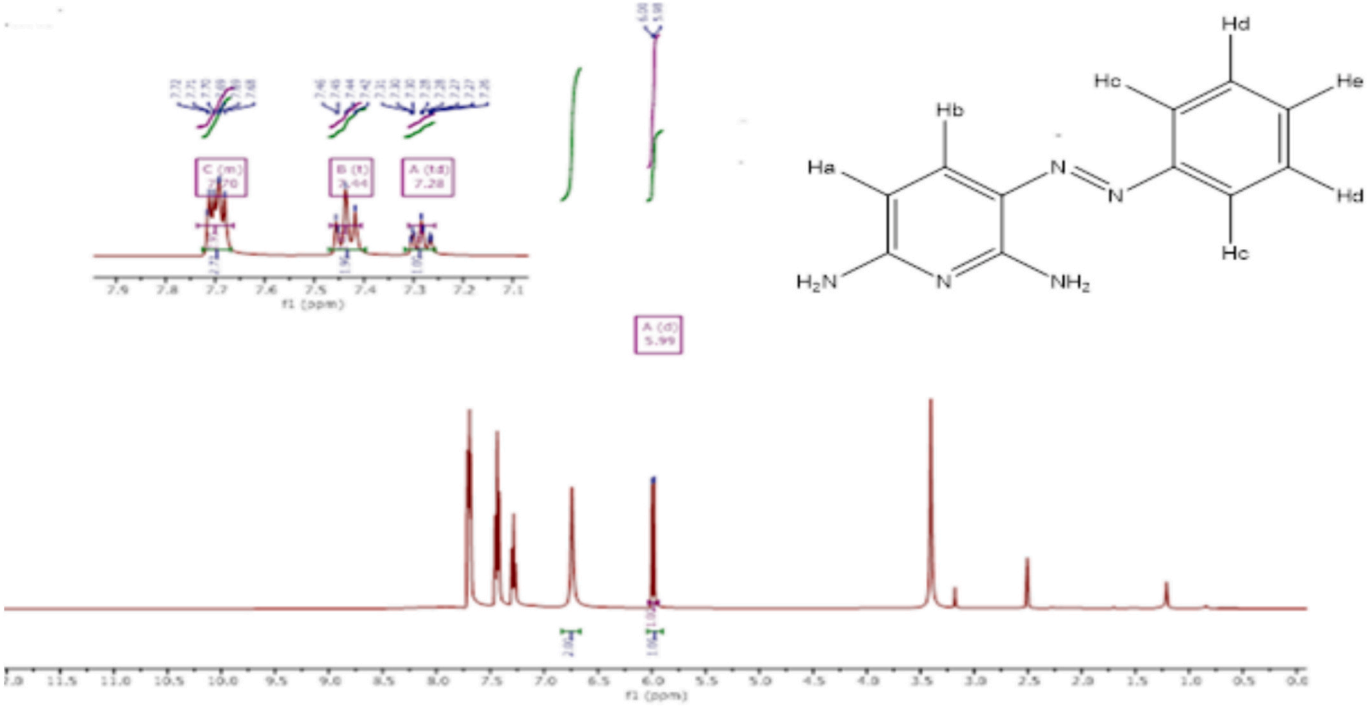

Fig. 3. The ^{1}HNMR spectra of free base phenazopyridine in DMSO-d_6 together with the molecular structure and proton assignments (Ha–He).

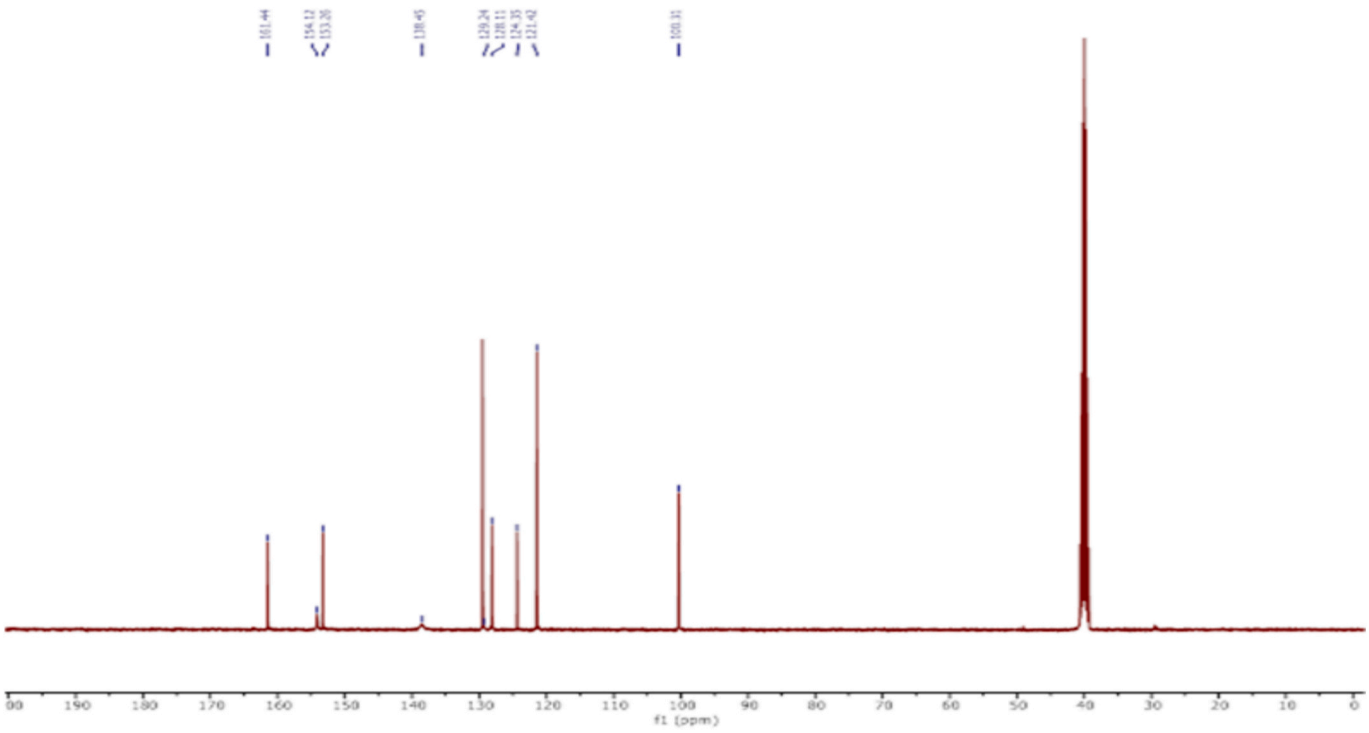

Fig. 4. The ^{13}CNMR spectra of free base phenazopyridine in DMSO-d_6.

effects, and some approximations of the computational procedure and the lack of explicit dynamic and intermolecular interactions in the calculations.

It is noteworthy that the experimental spectrum Fig. 5b shows much broader transitions than the discrete theoretical transitions, which can be explained by the presence of solvent interactions, vibrational broadening as well as inhomogeneous effects inherent to solution-state measurements. Irrespective of this expansion, the fact that the absorption maxima were very similar proves the accuracy of the TD-DFT method in forecasting the electronic structure of Phenazopyridine. Fig. 3a shows the experimental spectrum of absorption and the theoretically simulated spectrum in chloroform and Fig. 3b shows the experimental spectrum of absorption in thin films.

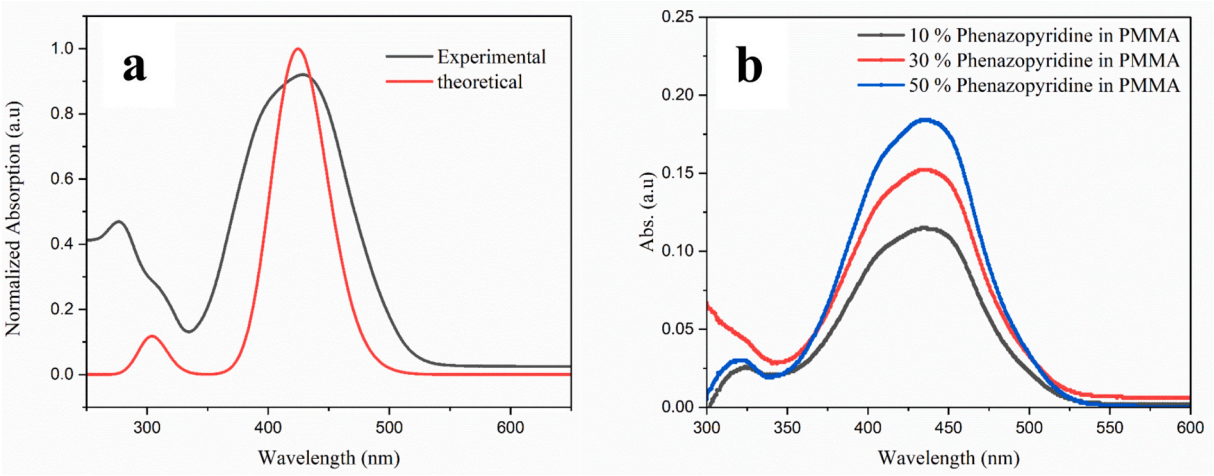

Fig. 5. Absorption spectra of phenazopyridine molecule as solution and thin film. a: theoretical and experimental absorption spectrum in chloroform, b: absorption spectrum for phenazopyridine doped PMMA with different doping ratio.

4.5. FMO Analysis and Global Reactivity Parameters

The electrons distribution of the frontier molecular orbitals (FMOs) of the Phenazopyridine molecule is shown in Fig. 6 with the red color and green color depicting the positive and negative phases of the molecular orbitals respectively. The HOMO-LUMO distribution shows clearly that the delocalization of the electrons occurs out of the electron-rich ring of the diaminobenzene (C1–C6, which can be associated with the -NH_2 donor group) to the electron-deficient ring of the pyridine (C9-C12, containing the N17) ring, mediated by the azo bridge (-N=N This geometrical segregation of the electron density validates the existence of an efficient donor–π–acceptor (D–π–A) framework, which is in line with the structural analysis presented above [27].

The energy gap (E_g) calculated 3.19 eV indicates moderate chemical reactivity and softness of the molecule, which allows π→π* and intramolecular charge transfer properties. Moreover, the HOMO-1 orbital is mainly concentrated on the amine-rich benzene ring whereas the LUMO+ 1 orbital is more delocalized throughout the entire molecular structure, further indicating the extended conjugation and charge transfer character [28,29].

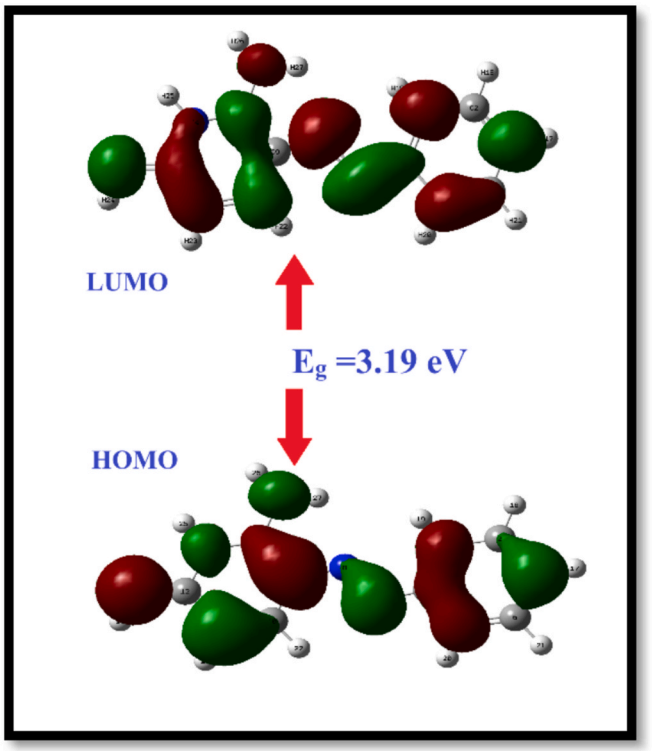

Fig. 6. FOM molecular orbitals (HOMO and LUMO) of Phenazopyridine calculated at the B3LYP levels.

The energy gap between the highest occupied molecular orbit (HOMO) and the lowest unoccupied molecular orbit (LUMO) from the CAM-B3LYP calculations was 5.58 eV. On a first glance, this value seems much higher than the experimental absorption energy of the major UV–Vis absorption band measured around 430 nm (2.88 eV). It is however not strictly correct to make a direct comparison between the HOMO–LUMO gap and the experimental energy of the optical absorption. The energy difference between frontier molecular orbitals in the ground state is a HOMO – LUMO gap, while the experimental absorption band is attributed to an electronic excitation process with excited state effects, electron correlation, orbital relaxation and excitonic interactions. Hence, the optical transition energies are better expressed in terms of the TD-DFT excitation energies and not in terms of the HOMO–LUMO gap.

Moreover, the CAM-B3LYP functional includes long-range correction and is proven to yield more accurate description of charge-transfer states, which may lead to larger orbital energy gaps than those of the conventional hybrid functionals. The experimentally observed absorption band at 430 nm is mainly attributed to π→π* and intramolecular charge transfer transitions in the donor-π- acceptor framework of Phenazopyridine as revealed by the TD-DFT calculations. Therefore, the HOMO–LUMO gap is not directly related to the optical absorption energy and should be considered as a qualitative measure of electronic stability and charge transfer ability of molecules.

The frontier molecular orbitals were analyzed (HOMO, LUMO) by use the B3LYP/6–311+G(d,p) and the CAM-B3LYP/6–311+G(d,p) basis set was utilized to calculating key parameters such as total energy, HOMO and LUMO energies, the energy gap (ΔE), ionization potential (I), electron affinity (A), absolute electronegativity (χ), absolute hardness (η), and softness (S). These properties provide a comprehensive understanding of the electronic behavior of Phenazopyridine, the table below summarizes these results [30].

Table 4 and 5 illustrates the electronic properties and the global reactivity descriptors of Phenazopyridine were studied with two different density functional theory (DFT) functionalities, i.e. B3LYP and CAM-B3LYP and the basis set used was 6311+G(d, p). It is found that the parameters calculated are highly dependent on the functional selected. The B3LYP procedure provides a less energy gap (ΔE = 3.19 eV), implying greater chemical reactivity and tenderness (S = 0.313 eV^{-1}).

Table 4
HOMO and LUMO energy, Energy gap, and oscillator strength for Phenazopyridine by using DFT/B3LYP and DFT/CAM-B3LYP.

functions	HOMO (eV)	LUMO (eV)	Energy Gap ΔE (eV)	Oscillator Strength *f*
B3LYP	−4.835466 eV	−1.641664 eV	3.193802 eV	1.244
CAM-B3LYP	−6.515498 eV	−0.937161 eV	5.578337 eV	1.180

Table 5
Global reactivity descriptors of phenazopyridine by using dft/b3lyp and dft/cam-b3lyp.

Descriptor	Relation	B3LYP	CAM-B3LYP
Chemical Potential μ (eV)	$\mu = (E_{LUMO} + E_{HOMO})/2$	−3.238565 eV	−3.726329 eV
Chemical Hardness η (eV)	$\eta = (E_{LUMO} - E_{HOMO})/2$	1.596901 eV	2.789169 eV
Chemical Softness S (eV^{-1})	$S = 1/(2\eta)$	0.313106 eV^{-1}	0.179265 eV^{-1}
Global Electrophilicity ω	$\omega = \mu^2/(2\eta)$	3.283955 eV	2.489188 eV
Nucleophilicity N (eV)	$N = E_{HOMO}$ (sample) − E_{HOMO} (TCE)	4.304843 eV	2.624812 eV

Conversely, the range-separated CAM-B3LYP functional that more correctly represents long-range interactions in conjugated systems predicts a larger energy gap (ΔE = 5.58 eV). The increased gap signifies increased kinetic stability and reduced reactivity as seen in a higher chemical hardness (η = 2.79 eV) and reduced softness (S = 0.179 eV^{-1}). Even though these differences exist, both methods identify Phenazopyridine as a strong electrophile with global electrophilicity indices (ω) of 3.28 eV and 2.49 eV of B3LYP and CAM-B3LYP, respectively, which is over the threshold of 1.5 eV. In both cases, the chemical potential (μ) is negative, which proves the stability of the molecule. On the whole, B3LYP gives a qualitative description of reactivity, but the CAM-B3LYP method would probably give a more quantitatively correct description of this extended π -conjugated system, which describes Phenazopyridine as a stable, but highly electrophilic compound.

4.6. Nonlinear Optical properties by quantum chemical calculations

The hyperpolarizability properties of the studied molecules were calculated using the finite field approach based on density functional theory (DFT) with the CAM-B3LYP functionals[31–34]. The results revealed high first hyperpolarizability (β) values, indicating a promising nonlinear optical (NLO) response. This behavior is attributed to the intramolecular charge transfer (ICT) mechanism between the donor and acceptor groups via the π-conjugated system, where this bridge acts as an effective channel for electron density redistribution under the influence of an external electric field. The hyperpolarizability values are extracted from the expansion of the molecular energy E(E) in a Taylor series with respect to the applied field strength, as shown in Equation (1), where the nonlinear terms directly contribute to determining the magnitudes of β and γ. The high β value confirms the role of the asymmetric electronic structure in enhancing the nonlinear optical properties, making these compounds potential candidates for applications in optoelectronic devices [35,36].

$$E(E) = E(0) - \mu_i F_i - \frac{1}{2!}\alpha_{ij}F_iF_j - \frac{1}{3!}\beta_{ijk}F_iF_jF_k - \frac{1}{4!}\gamma_{ijkl}F_iF_jF_kF_l - \cdots \quad (1)$$

Where E (0) is the unperturbed energy, μ the dipole moment, α the polarizability, and β/γ the first/second hyperpolarizabilities

$$\mu = \sqrt{\left(\mu_x^2 + \mu_y^2 + \mu_z^2\right)} \quad (2)$$

Polarizability and hyperpolarizability are given by:

$$\langle\alpha\rangle = \frac{\alpha_{xx} + \alpha_{yy} + \alpha_{zz}}{3} \quad (3)$$

$$\beta = \sqrt{\left(\beta_x^2 + \beta_y^2 + \beta_z^2\right)} \quad (4)$$

$$\langle\gamma\rangle = \frac{1}{5}\left(\gamma_{xxxx} + \gamma_{yyyy} + \gamma_{zzzz} + 2\gamma_{xxyy} + 2\gamma_{xxzz} + 2\gamma_{yyzz}\right) \quad (5)$$

It was performed through the Gaussian software package to study the nonlinear optical (NLO) properties (both static and frequency-dependent) of Phenazopyridine on a molecular level. All the calculations were carried out in the framework of the DFT using the CAM-B3LYP functional and basisbasing set set 6,311+G(d,p) basis set. The polarizability (a) and second hyperpolarizability (g) with a frequency of 0.0856 a.u. (wavelength 532 nm) were determined as summarized in Tables 6-8.

Strong dipole moments in molecular systems that have strong donor acceptor characteristics are generally characterized by effective intramolecular charge transfer. Here, the dipole moment (μ_{total}) of Phenazopyridine, calculated, is 1.5963 Debye (Table 6) which implies that there is moderate charge separation in the molecule.

The components of the tensors (α_{xx}, α_{yy}, α_{zz}) at ω = 0, while the dynamic polarizability α(−ω; ω) was evaluated at 0.0856 a.u. (λ = 532 nm). The results obtained indicate that the dynamic polarizability (87.03 $\times 10^{-2}$4 esu) is much greater than the static counterpart (12.29$\times 10^{-2}$4 esu), indicating how the molecular response is highly dependent on the applied electromagnetic field [30,35,36].

The first hyperpolarizability (β) tensor components and β_total values were computed under both static and dynamic conditions. The β_total values are 0.80, 8.33, and 30.83 × 10^{-30} esu for the static case, electro-optic effect (β(−ω; ω, 0)), and second harmonic generation (β(−2ω; ω, ω)), respectively. These values are significantly higher than that of urea (β ≈ 0.372 × 10^{-30} esu) and comparable to or exceeding those of p-nitroaniline (pNA), a standard NLO reference molecule [37]. The tensor components indicate a pronounced anisotropic response, suggesting that the dominant contribution corresponds to the primary intramolecular charge transfer pathway [24,36,38].

The second hyperpolarizability (γ) which is the third-order NLO response was also measured. The static value γ (0; 0,0,0) is 58.40 × 10^{-36} esu (Table 8), while the dynamic values increase significantly to 334.99 × 10^{-36} esu for the Kerr effect γ(−ω; ω, 0,0), and 4855.93 × 10^{-36} esu for electric-field-induced second harmonic generation (EFISH) γ(−2ω; ω, ω, 0). These values are quite high in comparison with most reported π-conjugated systems, which indicates a high degree of resonance enhancement and substantiates the promising performance of Phenazopyridine as a third-order NLO system.

Altogether, the acquired NLO parameters, when compared to the well-known reference molecules, as well as the systems that have been reported before, indicate that Phenazopyridine is a competitive candidate to be involved in the future advanced photonic and optoelectronic applications [38–41].

4.7. Nonlinear optical properties by Z scan technique

4.7.1. Open aperture results

The nonlinear optical (NLO) characteristics of Phenazopyridine were studied systematically under the Open Aperture (OA) Z-scan method, which quantifies the change in the transmitted intensity of a Gaussian laser beam through the sample in the absence of an aperture, thus giving direct information on the processes of nonlinear absorption in that

Table 6
The dipole momentum and static and frequency dependent(ω = 0.08564) polarizabilities of Phenazopyridine by using DFT/CAM-B3LYP method and 6–311 + G(d,p) basis set.

Dipole momentum (μ)		Polarizabilities (α)		
components	Values (Debye)		ω = 0	(−ω; ω)
μ_x	1.26314	α_{xx}	−261.987	675.275
μ_y	0.97357	α_{xy}	−180.984	−752.844
μ_z	0.06931	α_{yy}	308.871	183.433
μ_{total}	1.5963	α_{xz}	728.926	101.069
		α_{yz}	224.119	−388.224
		α_{zz}	201.853	903.219
		< α > a.u.	82.9123	587.309
		< α> esu	12.29 × 10−^{24}	87.0298 × 10−^{24}
		Δα a.u.	1455.74	1609.07

Table 7
The static and frequency dependent(ω = 0.08564) first order hyperpolarizabilities of Phenazopyridine by using DFT/CAM-B3LYP method and 6–311 + G(d,p)basis set.

Components	ω = 0	(−ω; ω, 0)	(−2ω; ω, ω)
		Electro-Optic Effect	SHG
β_{xxx}	98.0275	98.02750	314.1910
β_{xyy}	42.0347	14.93920	149.5200
β_{xzz}	86.6350	866.3500	3227.580
β_{yyy}	20.8648	2.086480	173.8440
β_{yzz}	10.4482	1044.820	3809.630
β_{yxx}	42.0347	42.03470	222.6220
β_{zzz}	12.4582	1245.820	5554.060
β_{zxx}	45.9745	459.7450	1337.500
β_{zyy}	57.6810	576.8100	1709.710
β_x	226.6972	979.3167	3691.291
β_y	73.34770	1107.719	4,206,096
β_z	116.1137	2282.375	8601.270
β_{total} a.u	92.21266	963.6916	3568.151
$\beta \times 10^{-30}$ esu	0.796625	8.325332	30.82526

Table 8
The static and frequency dependent(ω = 0.08564) second order hyperpolarizabilities of Phenazopyridine by using DFT/CAM-B3LYP method and 6–311 + G(d,p)basis set.

components	ω = 0	(−ω; ω, 0,0)	(−2ω; ω, ω,0)
	static	Keer effect	EFISH
γ_{xxxx}	53947.4	150,192	5.060830 x 10^6
γ_{yyyy}	75987.5	245,464	1.286610 x 10^7
γ_{zzzz}	15589.7	642,409	8.814700 x 10^6
γ_{xxyy}	36908.8	144,517	8.922090 x 10^6
γ_{xxzz}	66886.4	358,666	2.890210 x 10^4
γ_{yyzz}	87877.4	494,697	−3.333680 x 10^5
γ_{total} a.u	105774.0	606,765	8.795376 x 10^6
$\gamma \times 10^{-36}$ esu	58.3978	334.9950	4855.9269

sample but does not consider phase changes. Under this arrangement, the transmittance curve is symmetrical at the focal point which allows the separation between reverse saturable absorption (RSA) and saturable absorption (SA). The transmitted intensity is presented by [40,42,43].

$$T(z, s = 1) = 1 - \frac{q_o(z)}{2\sqrt{2}} \quad for\ |q_o(z) < 1| \tag{6}$$

where $q_0(z) = I_0 \beta L_{eff}/(1 + z^2 + z_0^2)$ with I_0 is the intensity of the laser beam at focus, β is the nonlinear absorption coefficient, z_0 is the Rayleigh range, L_{eff}=(1-exp(-αL))/α is the effective length of the sample (L is the sample length), and α is the linear absorption coefficient. The open-aperture Z-scan results are shown in Table 7 and Fig. 7. Fig. 7a corresponds to the Phenazopyridine solution, whereas Figs. 7b–d represent the Phenazopyridine/PMMA (Pe: PMMA) thin films with doping ratios of 10, 30, and 50, respectively.

From the results presented in Table 9 and Fig. 7, it is evident that the studied material exhibits reverse saturable absorption (RSA) behavior in both the solution and thin film forms. This nonlinear absorption behavior is characterized by a decrease in the transmittance near the focal point, the observed RSA behavior originates primarily from excited-state absorption (ESA), where the excited-state absorption cross-section exceeds the ground-state absorption cross-section. The extended π-conjugation, azo linkage, and donor–π–acceptor architecture of Phenazopyridine facilitate population of excited states and enhance ESA under laser excitation.

From the results presented above, it is evident that the investigated material exhibits reverse saturable absorption (RSA) behavior in both solution and thin film forms. In the case of the Phenazopyridine/PMMA thin films, a clear increase in the nonlinear absorption coefficient (β) is observed with increasing Phenazopyridine content relative to the PMMA matrix. The highest β value, corresponding to the largest doping ratio of 50%, was measured as 2.673×10^{-5} cm/kW. This enhancement can be attributed to the higher density of optically active molecules within the polymer host, which increases the probability of excited-state absorption and strengthens the nonlinear interaction with the incident laser beam. Such concentration-dependent behavior is commonly reported in organic dye–polymer composite systems, where increasing the dopant content enhances the nonlinear optical response due to improved light–matter interaction and more efficient intramolecular charge-transfer processes. These findings are consistent with previously reported results in the literature [40,44–47] and are summarized in Table 9.

Furthermore, the effect of incident laser intensity on the nonlinear absorption coefficient (β) was investigated to further explore the nonlinear response of the composite system and present in Fig. 8. The thin film that has a 50 percent doping ratio was chosen to be analyzed based on the results of the preceding analysis since it displayed the highest nonlinear optical response among the samples prepared. The measurements were done at three levels of laser which were 1, 1.8 and 2.76 kW/cm^2. The findings indicate that as the laser intensity is increased, there is a notable improvement in β which grows with the minimum intensity of 2.673×10^{-5} cm/kW to the maximum intensity of 1.344×10^{-4} cm/kW. This increase in β which depends on the intensity of the light is typical of RSA processes in which the absorption cross-section of the excited state is large compared to the absorption cross-section of the ground state, making the absorption of photons more intense with an increase in the incident photon flux. Table 10

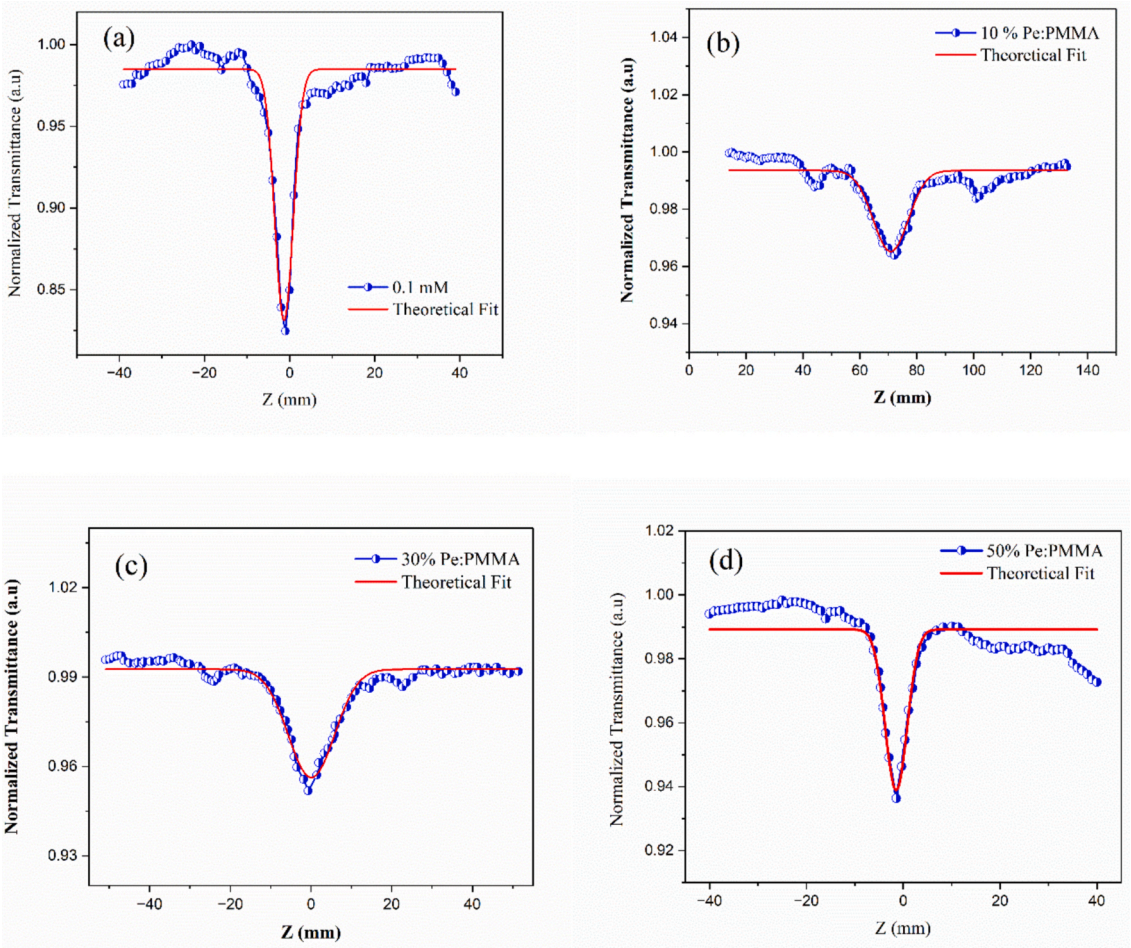

Fig. 7. Open aperture results for Phenazopyridine and Pe: PMMA at different doping ratio where a: 0.1 mM solution, b: 10 % Pe: PMMA, C: 30 % Pe: PMMA, d: 50 % Pe: PMMA.

Table 9
Linear and nonlinear absorption coefficient and nonlinear refractive index for Pe and Pe: PMMA 10, 30, and 50 % doping ratio.

NLO sample	α (cm^{-1})	ΔT_{Open}	β (cm /kW)	ΔT_{close}	Δ ∅ (rad)	n_2 (cm^2/ W)
0.1 mM	0.109	0.161	4.603x10^{-6}	1.9	5.3	−4.551 x10^{-7}
10%Pe: PMMA	0.132	0.031	1.397 x10^{-5}	0.523	1.464	−1.897 x10^{-6}
30%Pe: PMMA	0.191	0.041	1.851 x10^{-5}	0.558	1.562	−2.091 x10^{-6}
50%Pe: PMMA	0.307	0.059	2.673 x10^{-5}	0.74	2.07	−2.786 x10^{-6}

summarizes the nonlinear absorption parameters.

4.7.2. Close Aperture Results

The light exiting the nonlinear sample in the far-field was measured in the near-infrared with the closed-aperture (CA) Z- scan method by putting a 50 percent transmittance aperture in front of the detector. At incident laser intensity levels which are large enough to cause nonlinear optical behavior, the beam can either self-focus or self-defocus depending on the character of the nonlinearity of the material. The nonlinear refractive index is assessed using the normalized transmittance which is given as [43]:

$$T(z,\Delta\varnothing_o) = 1 - \frac{4\left(\frac{z}{z_o}\right)}{\left[\left(\frac{z^2}{z_o^2}\right)+9\right]\left[\left(\frac{z^2}{z_o^2}\right)+1\right]}\Delta\varnothing_0 \quad (7)$$

Where $\Delta\varnothing_o$ represents the on-axis phase shift at the focal point. This phase shift is related to the nonlinear refractive index n_2 through the relation:

$$n_2 = \frac{\Delta\varnothing_0}{I_0 L_{eff} \kappa} \quad (8)$$

Where k is the wave number ($2\pi/\lambda$).

The normalized transmittance curve has a typical pre-focal peak and then a post-focal valley which is characteristic of negative nonlinear refractive index ($n_2 < 0$). This effect is a consequence of self-defocusing mechanism where the refractive index is reduced with the increase in the incident light strength, and the beam tends to diverge in the area of focal point. This type of behavior indicates the negative optical nonlinearity inherent in the material and is consistent with all prepared samples of Pe and Pe: PMMA.

Fig. 9d shows the closed-aperture (CA) Z-scan results of the Pe solution at a concentration of 0.1 mM and an input intensity of 1.05 kW. The results of the corresponding Pe: PMMA thin films with the ratio of doping of 10 percent, 30 percent and 50 percent are in Fig. 7 a, b and c All the samples show a constant and stable arrangement of the peak and valley (P-V) configuration, which indicates the existence of negative nonlinear refraction in both the solution and the thin film system.

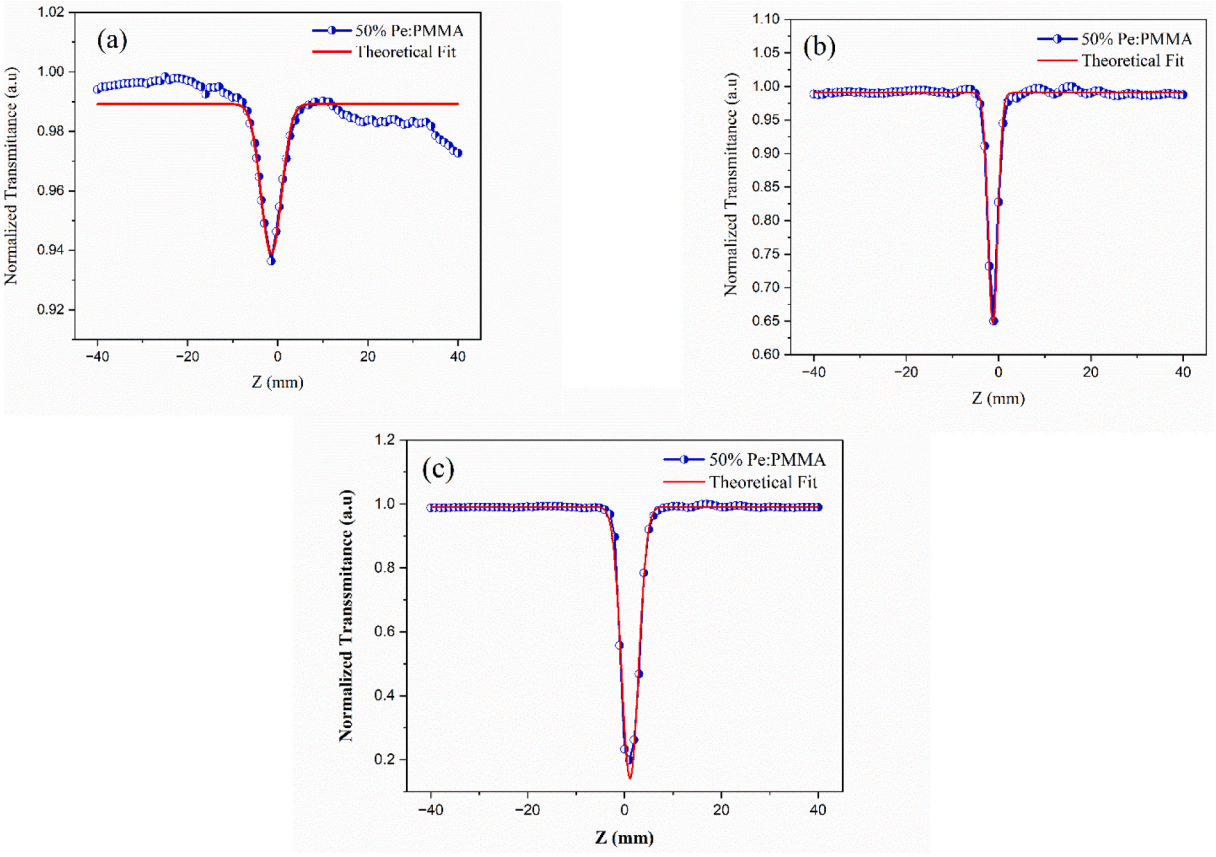

Fig. 8. O A Z-scan results for 50% Pe: PMMA at different Laser intensity, where a: 1.05, b: 1.8, and c: 2.76 kW/cm^2.

Table 10
Nonlinear absorption coefficient and nonlinear refractive index for 50% Pe: PMMA doping ratio at different incident laser power.

Power (mW)	Intensity (kW/cm^2)	ΔT $_{Open}$	β (cm/kW)	ΔT $_{close}$	Δφ (rad)	n_2 (cm^2/W)
9.5	1.05	0.059	2.673 x10^{-5}	0.74	2.07	−2.786 x10^{-6}
17	1.8	0.34	8.538 x10^{-5}	0.9	2.519	−1.893 x10^{-6}
25	2.76	0.787	1.344 x10^{-4}	1.461	4.08	−2.090 x10^{-6}

The values of n_2 were calculated using (8) and are summarized in Table 7. Fig. 9 shows the Z-scan results for the closed aperture. In general, the nonlinear refractive index of optical material can result from various contributions, such as electronic, molecular (orientational) and thermal contributions [48,49]. The nonlinear response observed for both Pe and Pe/PMMA is predominantly governed by thermal effects. Continuous-wave laser irradiation promotes absorption-induced heating, which produces spatial variations in the refractive index via the thermo-optic effect. Consequently, a negative nonlinear refractive index and self-defocusing behavior are generated. The diffraction-ring patterns and Z-scan results further support the predominance of thermally induced nonlinear refraction, in agreement with previous reports on related organic and polymer-based NLO systems. [46–50].

The observed from Fig. 10 is decrease in the nonlinear refractive index (n_2) with increasing incident laser intensity [51], accompanied by a simultaneous increase in the nonlinear absorption coefficient (β) under identical experimental conditions [52], is a manifestation of the competitive process between the refractive and absorptive nonlinear processes in the composite thin film. In the 50% doped sample, n_2 changed to 2.786 x10^{-6} cm^2/W at 1 kW/cm^2 to 2.09 x10^{-6} cm^2/W at 2.76 kW/cm^2, which shows the saturation of the refractive nonlinearity at higher excitation levels. This may be explained by the gradual filling of excited states in the π-conjugated framework of the Phenazopyridine molecules that hinders further polarization of the medium and decreases the efficiency of intensity-controlled modulation of the refractive index.

Conversely, nonlinear absorption coefficient (β) showed an upward trend with the laser intensity, indicating the occurrence of the excited-state absorption (ESA) and/or multi-photon absorption processes. In the Pe/PMMA system, azo (–N=N–) linkages, and extended π-electron conjugation enable effective transfer of charge and increases the likelihood of making an excited-state transition in the presence of high optical fields. Consequently, increased laser intensities enhance the existence of high levels of excited carriers, which further increases the chances of further photon absorption, leading to an enhancement in β[53,54].

Thus, when the intensity is high, nonlinear optical response of composite becomes more dominated by absorptive processes instead of refractive processes. This is typical of the azo dye-doped polymer systems, where the saturation of nonlinear refraction is coupled with the enhancement of nonlinear absorption caused by the enhancement of strong intramolecular charge transfer and excited-state dynamics [43,54,55].

4.8. *Diffraction ring patterns*

The experimental design was based on the Z-scan method, and a major adjustment to observe diffraction patterns in the far-field. The CW laser beam was directed on the NLO sample placed 5 cm in front of the lens (pre-focal region) where it needed to have sufficient intensity to induce spatial self-phase modulation with Kerr, though not to cause optical damage. The traditional Z-scan detector was substituted with a screen that lies 60 cm above the sample and digital camera to capture

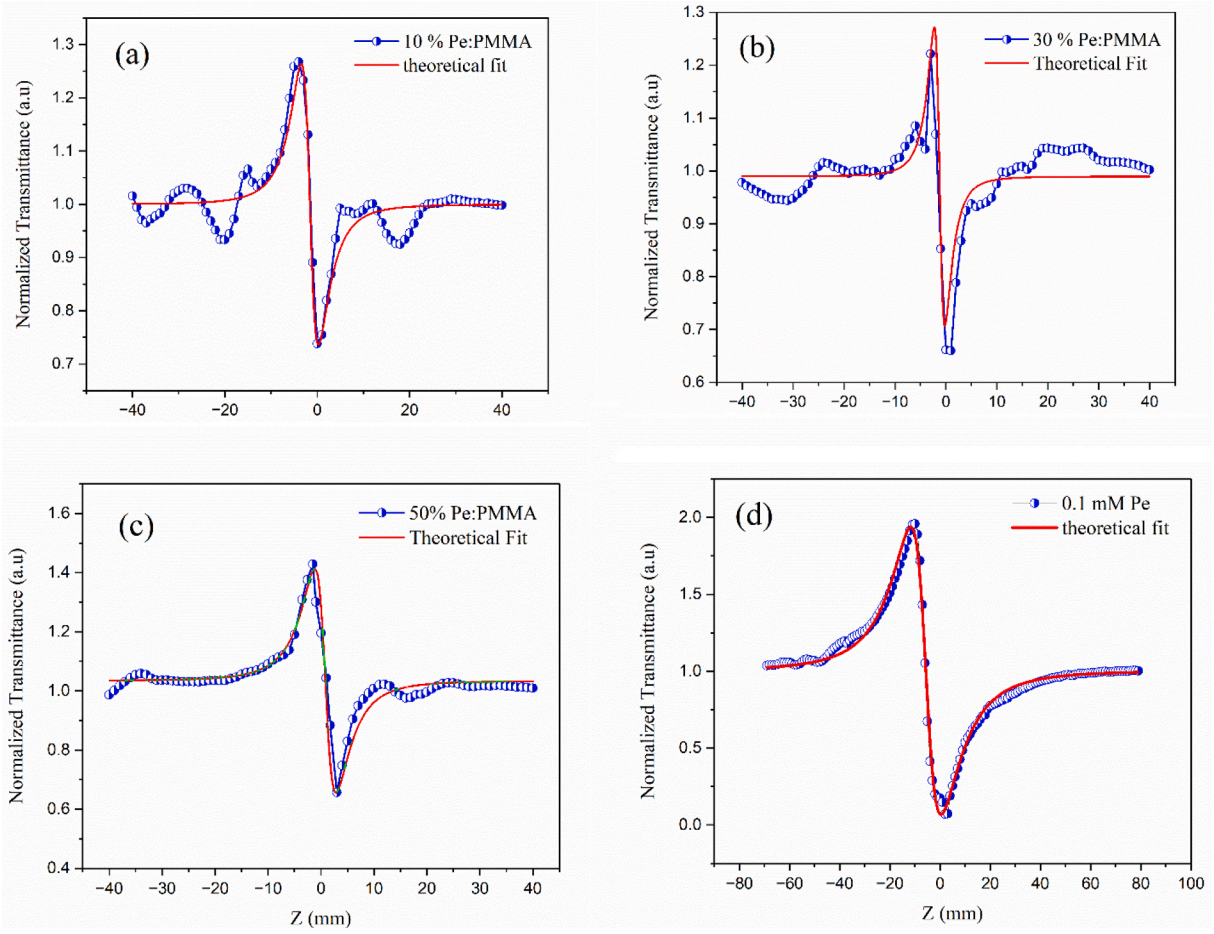

Fig. 9. (CA) Z-scan results for 0.1 mM Phenazopyridine (Pe) solution and Pe: PMMA at different doping ratio where a: 10 % Pe: PMMA, b: 30 % Pe: PMMA, c: 50 % Pe: PMMA, and d: 0.1 mM Pe solution.

the concentric diffraction ring pattern.

The observed number of rings (N) is directly proportional to the maximum nonlinear phase shift (Δ Φ) and the nonlinear refractive index (n_2) [56–60]:

$$N \cong \frac{\Delta\phi}{2\pi} \tag{9}$$

$$\Delta\phi = \frac{2\pi}{\lambda} L_{eff} n_2 I \tag{10}$$

Combining these yields the expression for n_2:

$$n_2 = \frac{\lambda N}{I L_{eff}} \tag{11}$$

Fig. 11 shows the self-diffraction ring patterns of the 0.1 mM Pe solution at with input power ranging from 1 mW to 55 mW, while Fig. 12 shows the self-diffraction ring patterns of the 50% Pe: PMMA film with input power ranging from 1 mW to 40 mW. It can be seen that the rings in each pattern of concentration start to increase from small rings to large number of rings as the power of laser beam increased.

The patterns of the far-field diffraction rings of the solution and the thin film samples are presented in Figs. 11 and 12 respectively. In the case of solution (Fig. 11), the diffraction rings were observed to form at an incident power as low as 5 m W and the number and diameter of the rings continued to increase with the increasing input power. The thin film (Fig. 12), to the contrary, did not show any rings until a certain power was reached; beyond this power, rings began to appear and quickly spread to the entire observation screen at 40 mW. The difference in thermal environments of the two sample forms is credited with this different threshold behavior. Linear absorption under constant -wave laser excitation results in localized heating, and the ensuing gradient in refractive index, controlled by the thermo-optic coefficient (dn/dT), causes the self- diffraction patterns to appear [61,62]. Effective heat loss in the solution due to convection and absence of rigid confinement allows a thermal lens to be built at relatively low powers in the solution. In the case of the thin film, though, the heat conduction is limited by both the substrate and the solid matrix, and more power is needed to create a high enough temperature gradient and thus a detectable thermal lens [56,61,63]. The nonlinear growth of the number and size of rings with incident power in both instances is typical of a thermally driven nonlinearity, which proves that the predominant mechanism is of thermal nature as opposed to electronic Kerr nonlinearity.

Fig. 13 presents the variation in the number of diffraction rings as a function of the incident laser power for the Phenazopyridine solution. Regarding to the Eq. (11), n_2 of the Pe solution and Pe: PMMA thin film can be determined and found to be equal 4.47×10^{-7} cm^2/W, and 1.92×10^{-7} cm^2/W respectively. This result is in a good agreement with data obtained through Z-scan experiment as seen in Table 7 and 8. The non-linearity of the analyzed samples was qualitatively and semi-quantitatively determined using a diffraction-ring method as a complementary technique. The analysis is performed under widely used conditions, using the thermal lens and spatial self-phase modulation models, according to which the number of diffraction rings is proportional to the accumulated nonlinear phase shift induced in the medium. When excited by continuous-wave laser, diffraction patterns observed are mainly controlled by thermally induced refractive-index gradients,

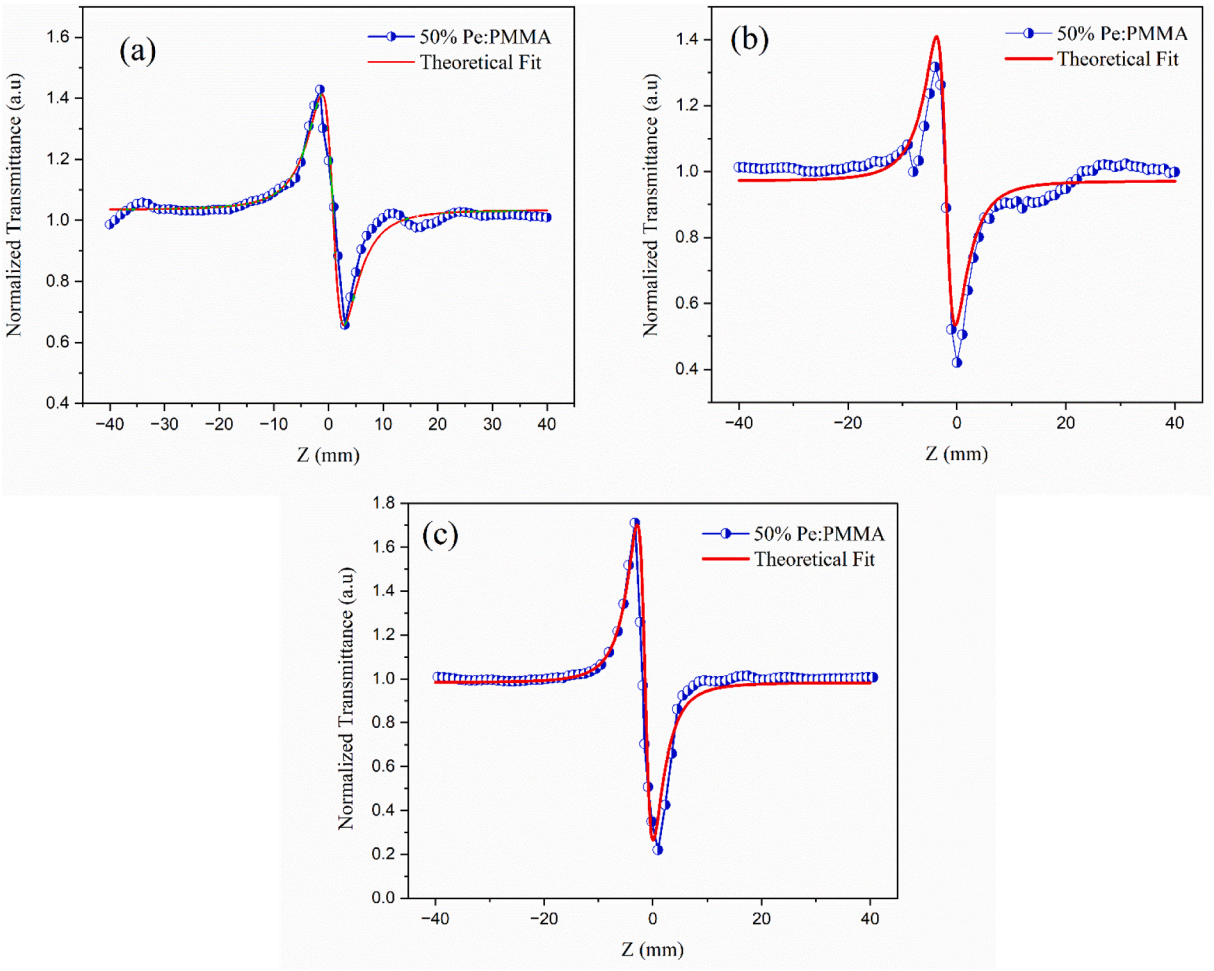

Fig. 10. C-A Z-scan results for 50% Pe: PMMA at different Laser intensity, where a: 1.05, b: 1.8, and c: 2.76 kW/cm2.

arising from linear absorption and the thermo-optic effect. Hence, the calculated n_2 values should be taken as effective nonlinear refractive indices in which the contributions of both electronic and thermal nonlinearities are included. The equations used are an approximation for thermally nonlinear media and have been extensively used for evaluation of organic dyes and polymer based nonlinear optical system under CW excitation, but still contain useful comparative information for the strength of the nonlinear response.

A clear quantitative discrepancy is observed between the nonlinear refractive index (n_2) values obtained from the Z-scan and diffraction ring techniques. This difference arises from the distinct physical mechanisms probed by each method. While the Z-scan technique probes the local intensity-dependent nonlinear response, including both electronic and thermal contributions under CW excitation, the diffraction ring method is more sensitive to cumulative thermal effects, particularly under continuous-wave excitation. Additionally, differences in interaction length, spatial averaging, and beam propagation further contribute to the variation in the measured n_2 values. Therefore, the discrepancy highlights the complementary nature of the two techniques rather than a contradiction, consistent with previous reports in nonlinear optical studies [56,57,59–65].

4.9. Optical limiting measurements

Because of the good nonlinear optical (NLO) characteristics of the analyzed material, defined by the values of the nonlinear refractive index (n_2) and nonlinear absorption coefficient (50% Pe: PMMA), it is necessary to examine the optical limiting behavior of both a solution form (Pe) and a thin film form (50% Pe: PMMA). A modified aperture Z-scan method was used to study the optical limiting behavior at a wavelength of 532 nm, with the sample fixed and the photodetector substituted with a power meter [66,67].

The optical limiting behavior of Pe solution and Pe: PMMA thin film at 532 nm is displayed as a function of time as shown in Fig. 14. In both instances, the power transmitted has a linear relationship with incident power at lower intensities, and then a nonlinear relationship at higher input powers, suggesting occurrence of optical limiting. One of the main parameters to evaluate the performance of optical limiters in the protection work is the limiting threshold.

The Pe solution has a lower limiting threshold (~7.5 mW) than the Pe: PMMA thin film (~12.6 mW), and thus, the Pe solution has a more efficient optical limiting response. Though the nonlinear absorption coefficient (β) of the thin film is bigger than that of the solution, the effective nonlinear interaction, which is dependent on both β, and the interaction length (L) determines the overall optical limiting behavior. The much greater thickness (solution was about 1 mm) of the solution than the thin film (about 60 μm) increases the cumulative nonlinear absorption ($\beta \times L$), which leads to a faster optical limiting.

Reverse saturable absorption (RSA) is the main regulator of the optical limiting behavior that is facilitated by the donor-π-acceptor structure and extended π-conjugation of Phenazopyridine, which facilitates intramolecular charge transfer and enhances excited-state absorption. The existence of azo and aromatic groups is also an addition to the π–π* transitions, and entrapment in the PMMA matrix stabilizes the nonlinear response. This process is in agreement with the measured nonlinear refractive index (n_2) and the threshold dependent formation of

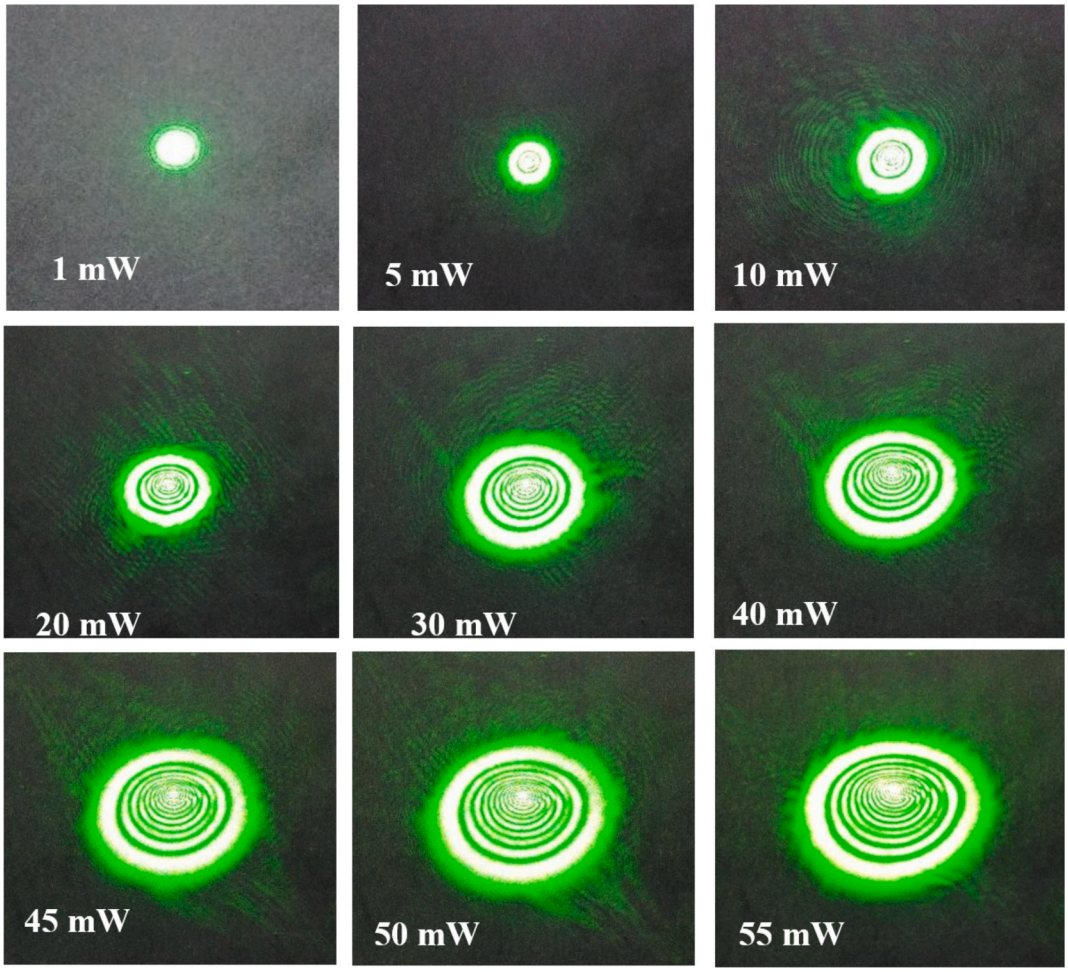

Fig. 11. Diffraction ring patterns of the Pe solution under input power from1 mW to 55 mW.

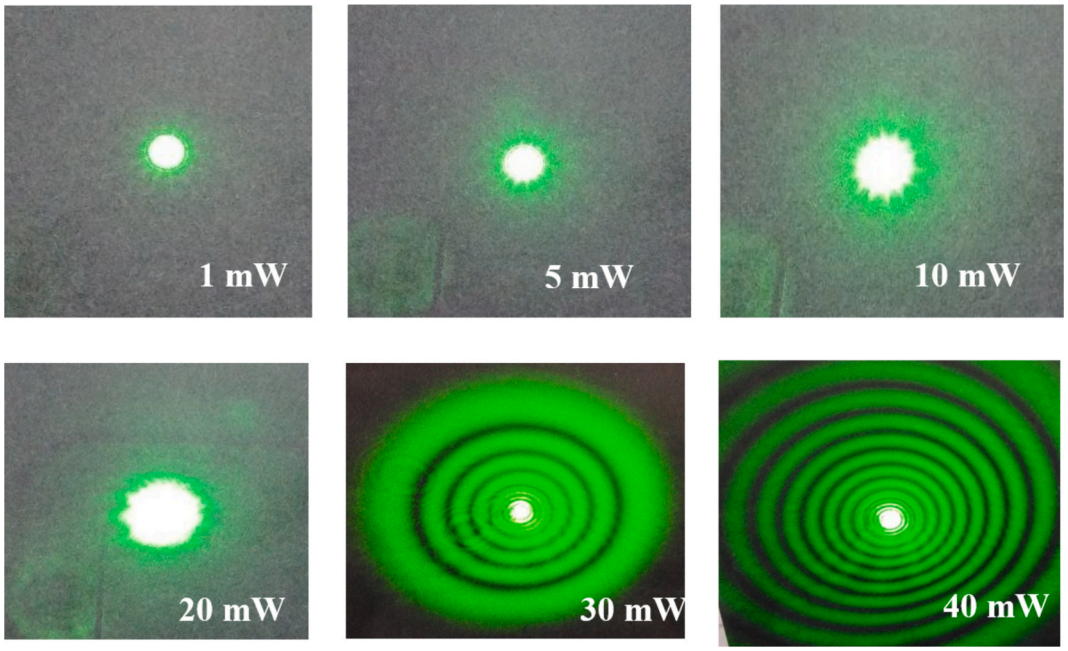

Fig. 12. Diffraction ring patterns of the 50% Pe: PMMA film under input power from1 mW to 40 mW.

diffraction rings where the appearance of rings at a certain input power is the confirmation of the prevailing role of thermally assisted nonlinear

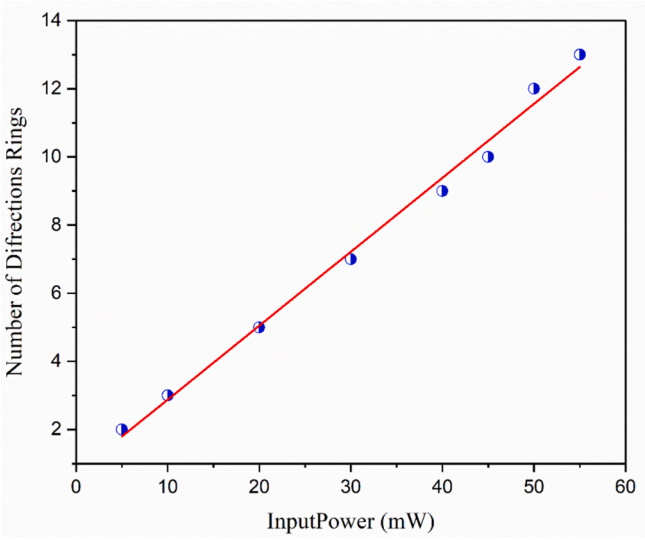

Fig. 13. Number of diffraction ring patterns of Pe solution under input power from1 mW to 55 mW.

absorption within the continuous-wave excitation [59,66–68].

In general, the findings show that optical limiting behavior is determined by a synergistic interplay of nonlinear optical properties intrinsic to the sample and extrinsic factors including the thickness of the samples and interaction length has the dominant role in defining the limiting behavior. There are a number of limitations to this work. The nonlinear behavior at different wavelengths cannot be analyzed, and the separation of thermal and electronic contributions cannot be achieved because using a single-wavelength continuous-wave (CW) laser does not allow the two to be separated. The response is thus largely thermal and this may be limiting in high-speed photonic devices where ultrafast electronic nonlinearities are needed. Moreover, the use of Phenazopyridine as a part of the PMMA matrix inhibits the movement of molecules and can affect the processes of charge transfer and the overall nonlinear functioning. Additionally, photostability and thermal stability of the composite over the long term were not studied and should be considered in the future.

In Table 11, the nonlinear optical parameters of the present Phenazopyridine/PMMA composites are compared with the NLO parameters of some representative organic dyes and polymer-based NLO materials. The nonlinear absorption coefficient (β) and nonlinear refractive index (n_2) obtained are similar or better than many of the previously reported systems based on azo-dyes. The reverse saturable absorption and self-defocusing properties of the 50 wt.% Phenazopyridine/PMMA film are particularly high, suggesting its application for optical limiting and photonic applications.

5. Conclusion:

Phenazopyridine was recovered and successfully incorporated in PMMA thin films and studied as a nonlinear optical material. Its donor–π–acceptor properties and charge transfer were confirmed by DFT calculations. The reverse saturable absorption and negative nonlinear refraction were observed in the Z-scan measurements and the nonlinear response was found to increase with the increase in Phenazopyridine content. The optical limiting performance was the best for the 50 wt.% film of Phenazopyridine/PMMA. The observed behavior when the laser is continuously excited was largely attributed to excited-state absorption and thermally induced nonlinear effects. The measured nonlinear optical parameters obtained are similar to those of other reported organic NLO compounds, indicating the feasibility of the recovered pharmaceutical compounds in the field of photonic and optical limiting applications.

The authors state that they have no competing financial interests or personal relationships with any of the authors of the papers referred to

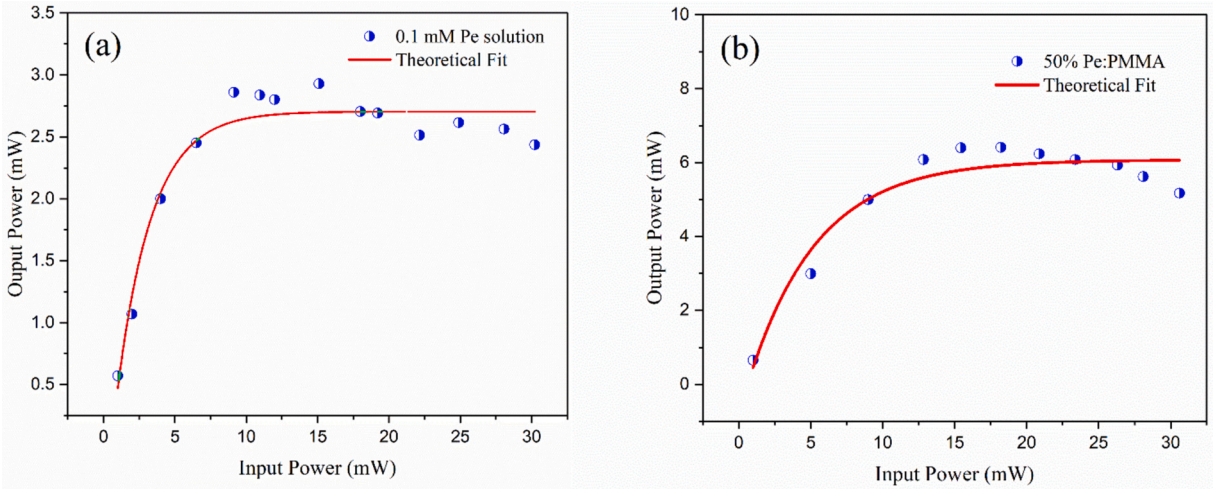

Fig. 14. Optical limiting results of the Pe solution at 0.1 mM concentrations, and 50% Pe: PMMA thin film.

Table 11
Comparison of the nonlinear optical parameters of Phenazopyridine/PMMA with selected organic NLO materials reported in the literature.

Material	λ (nm)	β (cm/W)	n_2 (cm^2/W)	NLO behavior	Ref.
Methyl Orange	532	$\sim10^{-5}$	$\sim10^{-7}$	RSA, self-defocusing	[41]
Organic azo dyes	532	10^{-6}–10^{-5}	10^{-7}–10^{-6}	RSA	[40]
Bixa Orellana dye/PMMA	532	10^{-6}	10^{-7}	RSA	[15]
Crystal Violet Polyamide	532	10^{-5}	10^{-6}	RSA, self-defocusing	[42]
Phenazopyridine solution (0.1 mM)	**532**	**4.60×10^{-6}**	**-4.55×10^{-7}**	**RSA, self-defocusing**	Present work
Phenazopyridine/PMMA (50 wt%)	**532**	**2.67×10^{-5}**	**-2.79×10^{-6}**	**RSA, self-defocusing**	Present work

in this paper that might have appeared to influence the outcome of this paper. There was no money provided to the author from any public, commercial or not-for-profit funding source to support this work.

CRediT authorship contribution statement

Raed K. Zaidan: Writing – original draft, Methodology, Formal analysis, Data curation, Conceptualization. **Basil A. Abdullah:** Writing – original draft, Supervision, Methodology, Formal analysis, Data curation, Conceptualization. **Mohammed T. Obeed:** Writing – review & editing, Formal analysis, Data curation. **Abeer Mohammed Jabbar:** Software, Methodology, Formal analysis. **Ali Qassim Abdullah:** Writing – review & editing, Validation, Supervision, Project administration, Formal analysis, Conceptualization.

Declaration of competing interest

The authors declare that they have no known competing financial interests or personal relationships that could have appeared to influence the work reported in this paper.

Acknowledgements

The authors extend their heartfelt gratitude to the Iraqi Ministry of Higher Education and Scientific Research (MOHER) as well as the Physics Department at the University of Basrah for their invaluable support.

Funding

"This research received no external funding"

Data availability

Data will be made available on request.

References

[1] Bhadoriya A, Patil B, Vinchurkar K, Mane S, Parambath A. Materials sustainability in the pharmaceutical industry. Sustainability & Circularity NOW 2024;1.
[2] Baroka IU. Pharmaceutical waste management: sources, environmental impacts, and sustainable solutions. Pharmacy Reports 2025;5:95.
[3] Hejna M, Kapuścińska D, Aksmann A. Pharmaceuticals in the aquatic environment: A review on eco-toxicology and the remediation potential of algae. Int. J. Environ. Res. Public Health 2022;19:7717.
[4] Lin H, Day DE, Stoffer JO. Optical and mechanical properties of optically transparent poly (methyl methacrylate) composites. Polym. Eng. Sci. 1992;32: 344–50.
[5] Tiwari A. Enhancing the Optical Properties of PMMA with Metamaterials: Mechanisms and Integration Techniques, International Journal of Multidisciplinary Research in Science. Engineering and Technology 2023;5:14098–107. https://doi.org/10.15680/ijmrset.2022.0512022.
[6] Biswas N, Umapathy S. Structures, vibrational frequencies, and normal modes of substituted azo dyes: infrared, Raman, and density functional calculations. J. Phys. Chem. A 2000;104:2734–45. https://doi.org/10.1021/jp9929263.
[7] Dalton L, Benight S. Theory-guided design of organic electro-optic materials and devices. Polymers. 2011;3:1325–51. https://doi.org/10.3390/polym3031325.
[8] Dalton LR, Sullivan PA, Bale DH. Electric field poled organic electro-optic materials: state of the art and future prospects. Chem. Rev. 2010;110:25–55.
[9] Zhang M, Xu X, Liu J, Jiang Y, Wang J, Dong N, et al. All-organic composite films for high flexibility and giant nonlinear optical limiting responses. ACS Appl. Mater. Interfaces 2022;14(2022):33787–96.
[10] Zollinger H. Color chemistry: syntheses, properties, and applications of organic dyes and pigments,3rd ed. John Wiley & Sons; 2003.
[11] Vijayakumar S, Adhikari A, Kalluraya B, Sharafudeen KN, Chandrasekharan K. Study of third-order optical nonlinearities of substituted hydrazones in PMMA. J. Appl. Polym. Sci. 2011;119:595–601.
[12] Ellen MacArthur Foundation. Towards the Circular Economy: Economic and Business Rationale for an Accelerated Transition. Cowes, UK: Ellen MacArthur Foundation; 2013.
[13] Burgueño-Tapia E, Mora-Pérez Y, Morales-Ríos MS, Joseph-Nathan P. 1H, 13C and 15N NMR assignments of phenazopyridine derivatives. Magn. Reson. Chem. 2005; 43:256–60. https://doi.org/10.1002/mrc.1542.
[14] Almosawe AJ, Saadon HL. Nonlinear optical and optical limiting properties of new structures of organic nonlinear optical materials for photonic applications. Chin. Opt. Lett. 2013;11:41902.
[15] Zongo S, Kerasidou AP, Sone BT, Diallo A, Mthunzi P, Iliopoulos K, et al. Nonlinear optical properties of poly(methyl methacrylate) thin films doped with Bixa Orellana dye. Appl. Surf. Sci. 2015;340:72–7. https://doi.org/10.1016/j.apsusc.2015.02.161.
[16] Kaliramna S, Dhayal SS, Kumar N. Fabrication of PMMA thin film and its optical and photocatalytic activity. Mater. Today Proc. 2022;69:42–6. https://doi.org/10.1016/j.matpr.2022.08.327.
[17] A.A. Said, M. Sheik-Bahae, T.H. Wei, J. Young, D.J. Hagan, M.J. Soileau, E.W. Van Stryland, z-scan: a simple sensitive technique for measuring refractive nonlinearities, in: Annual Meeting Optical Society of America, Optica Publishing Group, 1989: p. TUY3. https://doi.org/10.1364/OAM.1989.TUY3.
[18] M.J. Frisch, G.W. Trucks, H.B. Schlegel, et al., Gaussian 16, Revision C.01, Gaussian Inc., Wallingford, CT, USA, 2016.
[19] Binning Jr RC, Curtiss LA. Compact contracted basis sets for third-row atoms: Ga–Kr. J. Comput. Chem. 1990;11:1206–16.
[20] McGrath MP, Radom L. Extension of Gaussian-1 (G1) theory to bromine-containing molecules. J. Chem. Phys. 1991;94:511–6. https://doi.org/10.1063/1.460367.
[21] Curtiss LA, McGrath MP, Blaudeau JP, Davis NE, Binning RC, Radom L. Extension of Gaussian-2 theory to molecules containing third-row atoms Ga-Kr. J. Chem. Phys. 1995;103:6104–13. https://doi.org/10.1063/1.470438.
[22] Dennington R, Keith TA, Millam JM. GaussView, Version 6. Shawnee Mission, KS, USA: Semichem Inc.; 2016.
[23] Marques MAL, Maitra NT, Nogueira FMS, Gross EKU, editors. Fundamentals of Time-Dependent Density Functional Theory. Berlin: Springer; 2012.
[24] Dreuw A, Head-Gordon M. Failure of time-dependent density functional theory for long-range charge-transfer excited states: the zincbacteriochlorin–bacteriochlorin and bacteriochlorophyll–spheroidene complexes. J. Am. Chem. Soc. 2004;126: 4007–16.
[25] Yanai T, Tew DP, Handy NC. A new hybrid exchange–correlation functional using the Coulomb-attenuating method (CAM-B3LYP). Chem. Phys. Lett. 2004;393:51–7. https://doi.org/10.1016/j.cplett.2004.06.011.
[26] Y. Akkaya, K. Balcı, Y. Gören, S. Akyüz, Molecular Structure and Vibrational Characteristics of Phenazopyridine Molecule: The IR, Raman and DFT Studies, Proc. 5th Int. Conf. Advanced Vibrational Spectroscopy (ICAVS-5), Melbourne, Australia, 12–17 July 2009, 151.
[27] Osman OI. DFT study of the structure, reactivity, natural bond orbital and hyperpolarizability of thiazole azo dyes. Int. J. Mol. Sci. 2017;18. https://doi.org/10.3390/ijms18020239.
[28] Biswal D, Jha A, Sen A. Screening donor and acceptor groups for organic azo-based dyes for dye sensitized solar cells. J. Mol. Struct. 2021;1228. https://doi.org/10.1016/j.molstruc.2020.129776.
[29] Galli S, Masciocchi N, Sironi A. Ab initio X-ray powder diffraction characterisation of molecule-based magnetic materials, in. Journal of Physics and Chemistry of Solids 2004:693–6. https://doi.org/10.1016/j.jpcs.2003.11.001.
[30] Muhammad H, et al. An Interesting Behavior and Nonlinear Optical (NLO) Response of Hexamolybdate Metal Cluster: Theoretical Insight into Electro-Optic Modulation of Hybrid Composites. Journal of Cluster Science 2017;28:2693–708.
[31] Olsen J, Jørgensen P. Linear and nonlinear response functions for an exact state and for an MCSCF state. J. Chem. Phys. 1984;82:3235–64. https://doi.org/10.1063/1.448223.
[32] Umar A, Yaqoob J, Khan MU, Riaz Hussain A, Alhadhrami ASA, Almalki. Muhammad Ramzan Saeed Ashraf Janjua, Doping of superalkali and superhalogen on graphene quantum dot surfaces to enhance nonlinear optical response: An efficient strategy for fabricating novel electro-optical materials. J. Phys. Chem. Solids 169 2022:110859.https://doi.org/10.1016/j.jpcs.2022.110859.
[33] Rice JE, Handy NC. The calculation of frequency-dependent polarizabilities as pseudo-energy derivatives. J. Chem. Phys. 1991;94:4959–71. https://doi.org/10.1063/1.460558.
[34] Janjua MRSA, Guan W, Yan L, Su Z-M, Karim A, Akbar J. Quantum chemical design for enhanced second-order NLO response of terpyridine-substituted hexamolybdates. Eur. J. Inorg. Chem. 2010;2010:3466–72. https://doi.org/10.1002/ejic.201000428.
[35] Thanthiriwatte KS, de Silva KMN. Non-linear optical properties of novel fluorenyl derivatives: ab initio quantum chemical calculations. J. Mol. Struct. THEOCHEM 2002;617:169–75. https://doi.org/10.1016/S0166-1280(02)00419-0.
[36] Ghanavatkar CW, Mishra VR, Sekar N. Review of NLO phoric azo dyes – Developments in hyperpolarizabilities in last two decades. Dyes and Pigments 2021;191. https://doi.org/10.1016/j.dyepig.2021.109367.
[37] Warren WS. Effects of arbitrary laser or NMR pulse shapes on population inversion and coherence. J. Chem. Phys. 1984;81:5437–48. https://doi.org/10.1063/1.447644.
[38] Boyd RW. Nonlinear Optics. Academic Press; 2020.
[39] Albert IDL, Morley JO, Pugh D. Optical nonlinearities in azoarenes. J. Phys. Chem. 1995;99:8024–32. https://doi.org/10.1021/j100020a023.
[40] Motiei H, Jafari A, Naderali R. Third-order nonlinear optical properties of organic azo dyes by using strength of nonlinearity parameter and Z-scan technique. Opt. Laser Technol. 2017;88:68–74. https://doi.org/10.1016/j.optlastec.2016.09.011.
[41] Del Nero J, De Araujo RE, Gomes ASL, De Melo CP. Theoretical and experimental investigation of the second hyperpolarizabilities of methyl orange. Journal of Chemical Physics 2005;122. https://doi.org/10.1063/1.1860372.
[42] Almusawe AJ, Rahma MA, Saadon HL, Abdullah AQ, Marhoon AF. Optical nonlinear properties of a new polyamide from crystal violet terephthalate. Phys. Scr. 2024;99:115519. https://doi.org/10.1088/1402-4896/ad81c4.

[43] Sheik-Bahae M, Said AA, Wei T-H, Hagan DJ, Van Stryland EW. Sensitive measurement of optical nonlinearities using a single beam. IEEE J. Quantum Electron. 1990;26:760–9.
[44] Obeed MT, Alaridhee TA, Abdullah RM, Badran HA, Abul-Hail RC, Hasan HA, et al. Studies of third order nonlinearity and thermal diffusivity of C3OC dye using thermal lens technique. Results Phys. 2024;66. https://doi.org/10.1016/j.rinp.2024.108001.
[45] H.A. Bdran, R.C.H. Abul-Hail, M.T. Obeed, Study on effect of gamma radiation on some linear and nonlinear properties of Pyronine y, in: AIP Conf. Proc., American Institute of Physics Inc., 2020. https://doi.org/10.1063/5.0027452.
[46] Almusawe AJ, Rahma MA, Mohammed EA, Saadon HL. Application of Z-scan technique for the study of nonlinear optical properties of BCP/MEH-PPV. Nonlinear Optics, Quantum Optics: Concepts in Modern Optics 2020;52:253–64.
[47] Al I-A-D-H, Saidi HFH, Sleem N. Preparation of poly(3HT-co-TH)/PMMA polymer blend films and study of their optical properties. Int. J. Eng. Trends Technol. 2020;68:72–6.
[48] de Nalda R, del Coso R, Requejo-Isidro J, Olivares J, Suarez-Garcia A, Solis J, et al. Limits to the determination of the nonlinear refractive index by the Z-scan method. J. Opt. Soc. Am. B 2002;19:289–96. https://doi.org/10.1364/JOSAB.19.000289.
[49] Falconieri M. Thermo-optical effects in Z-scan measurements using high-repetition-rate lasers. J. Opt. A: Pure Appl. Opt. 1999;1:662–7.
[50] Tremblay M, et al. Z-scan studies of refractive index changes in azo-dye-doped PMMA films. Proc. SPIE 1998;3294.
[51] Dhami S, Kumar Y, Singh Y, Pradhan AK, Datta PK, Thomas KRJ, et al. Comprehensive investigation of the ultrafast excited state dynamics and nonlinear optical properties of pyrene derivatives with different push–pull properties. Physical Chemistry Chemical Physics 2025;27:8910–9.
[52] Sadigh MK, Zakerhamidi MS. Solvent polarity sensitive characteristics of various tautomers of azo compounds: Linear and nonlinear optical properties. Spectrochim. Acta A Mol. Biomol. Spectrosc. 2020;239.
[53] Yang L, Wang G, Wang J, Wang G, Xu Z. Spectroscopic properties of azo-dye doped PMMA films studied by multi-photon absorption. Optik 2002;113(4):189–91.
[54] S. Liu, J.H. Lin, J.H. Lin, V.M. Churikov, J.T. suen Lin, T.H. Huang, C.C. Hsu, Photoisomerization-induced change of nonlinear absorption in azo-dye doped polymethylmethacrylate thin films, Opt. Commun. 236 (2004) 33–43. https://doi.org/10.1016/j.optcom.2004.03.013.
[55] Papagiannouli I, et al. Third-order nonlinear optical response of push–pull azobenzene polymers. Chem. Phys. Lett. 2012;554:107–12.
[56] Yang X, Li D, Li Q, Meng X. Spatial self-phase modulation of a Gaussian beam transmitted through a ferrofluid. Appl. Opt. 2020;59:10069–75. https://doi.org/10.1364/AO.406296.
[57] Abdullah RM, Obeed MT, Sweah ZJ, Badran HA, Abul-Hail RC, Hamzah MQ. Self-Diffraction Characterization and Optical Limiting Behavior of the PAni/PVA Nanofiber. Polymer Science - Series A 2024;66:348–62. https://doi.org/10.1134/S0965545X24600960.
[58] Ogusu K, Kohtani Y, Shao H. Laser-induced diffraction rings from an absorbing solution. Opt. Rev. 1996;3:232–4.
[59] Alizadeh A, Rajabi Y, Zare EN. Investigation of the nonlinear optical properties of sodium alginate-grafted-poly(3-aminophenol)/metal–organic framework nanocomposite: Possible application in all-optical switching. Alexandria Engineering Journal 2025;114:453–62. https://doi.org/10.1016/j.aej.2024.11.091.
[60] Mahdy A. Furat A. Al-Saymari, Investigation of nonlinear optical properties of Sudan red G dye solutions using diffraction rings patterns and z-scan technique, University of Thi-Qar Journal of Science 2024;11:116–24. https://doi.org/10.32792/utq/utjsci/v11i2.1265.
[61] Shabeeb GM, Emshary CA, Hassan QMA, Sultan HA. Investigating the nonlinear optical properties of poly eosin-Y phthalate solution under irradiation with low power visible CW laser light. Physica B Condens. Matter 2020;578. https://doi.org/10.1016/j.physb.2019.411847.
[62] Dabby FW, Gustafson TK, Whinnery JR, Kohanzadeh Y, Kelley PL. Thermally self-induced phase modulation of laser beams. Appl. Phys. Lett. 1970;16:362–5. https://doi.org/10.1063/1.1653226.
[63] Callen WR, Huth BG, Pantell RH. Optical patterns of thermally self-defocused light. Appl. Phys. Lett. 1967;11:103–5. https://doi.org/10.1063/1.1755036.
[64] Tuma FA, Obeed MT, Jari AA, Ali Badran H, Alaridhee TA. Effect of gamma ray on self-induced diffraction patterns of organic compound Poly (methyl-methacrylate films. Results Phys. 2023;52. https://doi.org/10.1016/j.rinp.2023.106858.
[65] Zidan MD, Al-Ktaifani MM, M.S. EL-Daher, A. Allahham, A. Ghanem. Diffraction ring patterns and nonlinear measurements of the Tris(2′,2-bipyridyl) iron (II) tetrafluoroborate. Opt. Laser Technol. 2020;131. https://doi.org/10.1016/j.optlastec.2020.106449.
[66] Hassan QMA, Emshary CA, Sultan HA. Investigating the optical nonlinear properties and limiting optical of eosin methylene blue solution using a cw laser beam. Phys. Scr. 2021;96:95503. https://doi.org/10.1088/1402-4896/ac0868.
[67] Abed WJ, Mahdi ZF, Aboud LH. "Optical limiting properties of Acridine dye solution and doped PMMA, Al2O3 nanoparticles using Nd-YAG laser." Academic Research. International 2014;5(6):61.
[68] Mathews SJ, Kumar SC, Giribabu L, Rao SV. Nonlinear optical and optical limiting properties of phthalocyanines in solution and thin films of PMMA at 633 nm studied using a cw laser. Mater. Lett. 2007;61:4426–31. https://doi.org/10.1016/j.matlet.2007.02.034.